Geophys. J. Int. (2004) **159,** 688–702 doi: 10.1111/j.1365-246X.2004.02409.x

Numerical modelling method for wave propagation in a linear viscoelastic medium with singular memory

Jian-Fei Lu[1,2] and Andrzej Hanyga[2]

[1] *Mathematics and Physics Institute of Jiangsu University, Zhenjiang, Jiangsu* 212013, *China. E-mail: ljfdoctor@yahoo.com*
[2] *Institute of Earth Science, University of Bergen, Allegaten* 41, *Bergen* N5007, *Norway. E-mail: andrzej.hanyga@geo.uib.no*

Accepted 2004 June 19. Received 2004 March 4; in original form 2003 October 6

SUMMARY

A numerical modelling method for wave propagation in a linear viscoelastic medium with singular memory is developed in this paper. For a demonstration of the method, the Cole–Cole model of viscoelastic relaxation is adopted here. A formulation of the Cole–Cole model based on internal variables satisfying fractional relaxation equations is applied. In order to avoid integrating and storing of the entire history of the variables, a new method for solving fractional differential equations of arbitrary order based on a set of secondary internal variables is developed. Using the new method, the velocity–stress equations and the fractional relaxation equations are reduced to a system of first-order ordinary differential equations for the velocities, stresses, primary internal variables as well as the secondary internal variables. The horizontal spatial derivatives involved in the governing equations are calculated by the Fourier pseudo-spectral (PS) method, while the vertical ones are calculated by the Chebychev PS method. The physical boundary conditions and the non-reflecting conditions for the Chebychev PS method are also discussed. The global solution of the first-order system of ordinary differential equations is advanced in time by the Euler predictor–corrector methods. For the demonstration of our method, some numerical results are presented.

Key words: Cole–Cole law, fractional derivative, pseudo-spectral method, singular memory, viscoelastic, wave-propagation modelling.

1 INTRODUCTION

The real medium of the Earth is different from an ideal elastic solid in many respects. Consequently, seismic wave propagation in the Earth has been considered to be anelastic for a very long time. Compared with the elastic case, the wave motion in an anelastic medium has many different properties. For example, wave attenuation and dispersion significantly affect the amplitude and the traveltime of the wave field. Also, the physical characteristics of the plane wave on the plane boundary separating two viscoelastic media are different from those of the elastic case: a special type of wave, called a generalized inhomogeneous wave can be generated near the interface (Borcherdt 1982; Borcherdt & Wenneberg 1985). Therefore, an accurate wavefield simulation method should be able to account for the effects of attenuation and dispersion.

Up to now, there have been many papers concerning numerical wavefield modelling in a heterogeneous viscoelastic medium (Day & Minster 1984; Emmerich & Korn 1987; Carcione *et al.* 1988; Xu & Mcmechan 1995). However, the investigations are mainly limited to the generalized standard linear viscoelastic solid. For the generalized standard linear viscoelastic solid, the complex modulus belongs to the rational function. By using Padé approximation, the time convolution involved in the constitutive relation can be evaluated by a series of internal variables satisfying the first-order differential equation (Day & Minster 1984; Emmerich & Korn 1987). Alternatively, because the stress relaxation function of the generalized standard linear solid is of exponential type, the convolution in the constitutive relation can be eliminated by introducing internal variables, which satisfy the first-order ordinary differential equation (Carcione *et al.* 1988; Xu & Mcmechan 1995). Exponential-type stress relaxation functions and their derivatives are bounded at the initial time. However, both creep tests (Rabotnov 1980) and vibration tests (Nolte *et al.* 2003) suggest that the derivatives of stress relaxation functions have an asymptotic behaviour const $\times\, t^{-\alpha}$ at $t \to 0$, where $0 < \alpha < 1$. In this paper, a viscoelastic medium with a viscoelastic kernel having a singularity const $\times\, t^{-\alpha}$ at $t \to 0$ is called a singular memory viscoelastic medium. Unlike the standard linear solid, the complex modulus of singular memory viscoelastic medium is not the rational function. Also, in general, the stress relaxation function and its derivative of the singular memory viscoelastic medium cannot be represented in terms of the exponential function. As a result, the convolution in the constitutive relation of the heterogeneous viscoelastic medium with singular memory cannot be eliminated by the method used in the case of the generalized standard linear viscoelastic solid. Consequently, if the convolutions involved in the constitutive relations are evaluated by direct

integration method, then, the wavefield simulation for the singular memory viscoelastic medium requires storing and integrating with the entire history of the corresponding variables. The difficulty persists as a result of the non-local property of the fractional derivatives, if the convolutions in constitutive equations with singular kernels are expressed in terms of fractional derivatives (Glöckle & Nonnenmacher 1991; Friedrich & Braun 1994).

A commonly accepted seismic attenuation model is based on the assumption of constant Q. There are, however, only two models of constant Q in wave propagation. The Caputo–Kjartansson model (Kjartansson 1979) is rigorous but it implies an infinite speed of wave propagation. Futterman's model (Futterman 1962) is cumbersome and requires two arbitrary cut-offs, at high and low frequencies. Without the high-frequency cut-off, it violates the conditions of hyperbolicity and causality. It was aptly reformulated by Strick (1970). In this form it is equivalent to a power law with an exponent $1-\varepsilon$, with ε treated as an infinitesimal quantity. However, according to the Paley–Wiener theorem (Papoulis 1962), the resulting solution (for a delta input pulse) violates causality. In contrast to the power law, the corresponding stress relaxation function is rather complicated, whence it is useless for numerical implementation. On the other hand, the Cole–Cole model (Cole & Cole 1941) has been validated experimentally in both quasi-static and vibrations experiments (Nolte *et al.* 2003). It has been pointed out in several papers, for example Bagley & Torvik (1986) and Soula *et al.* (1997), that the Cole–Cole model fits experimental data over several decades of frequency. Experimental evidences in rock physics (Jones 1986; Batzle *et al.* 2001) also point to the Cole–Cole type behaviour. Furthermore, the Cole–Cole relaxation model has many advantages over other models. In particular, the Cole–Cole relaxation model is compatible with a finite speed of wave propagation. The Cole–Cole model has a very economical parametrization: it only involves four parameters. Also, a constant-Q model can be approximated by a Cole–Cole model with a small value of the exponent (Hanyga 2003a). The Cole–Cole model and Strick's version of Futterman's constant-Q model are singular memory models. This implies wave front smoothing and pulse delay (Hanyga & Seredyńska 1999), called by Strick (Strick 1970) the pedestal effect.

The purpose of this contribution is to develop a new efficient method for wavefield simulation of the heterogeneous isotropic viscoelastic medium with singular memory. The proposed method avoids the storage and integration of the entire history of physical variables. For the demonstration of the method, the Cole–Cole model (Cole & Cole 1941) is chosen in the paper (Section 2). The velocity–stress formulation involving internal variables is derived for the Cole–Cole viscoelastic medium. Following Hanyga (2003b), the fractional differential equations for the relaxation of the internal variables are derived. A direct discretization of the fractional relaxation equations by the Grunwald–Letnikov approximation (Podlubny 1998) or by the FraPECE method (Diethelm *et al.* 2002) is prohibitively expensive in the context of partial differential equations. Consequently, a new method for solving fractional differential equations in time domain is developed in Section 3. The method avoids integrating and storing the entire history of the internal variables. Using the method, the fractional differential equations for the internal variables are reduced to a system of first-order ordinary differential equations, which are satisfied by the primary and secondary internal variables. The numerical scheme is based on the first-order ordinary differential equations for the primary and secondary internal variables as well as the usual equations for velocity and stress (Section 4.1). The spatial derivatives of the velocities and stresses in the horizontal direction are calculated by the Fourier pseudo-spectral (PS) method, while the vertical ones are calculated by the Chebychev PS method (Section 4.2). The physical boundary conditions and the non-reflecting conditions for Chebychev PS method are discussed in Section 4.3. Combined with initial conditions and appropriate boundary conditions, the resulting first-order ordinary differential equations can be solved in the time domain. The global solution of the total system is advanced in time by the Euler predictor–corrector method. For the demonstration of our method, some numerical results are presented in Section 5.

2 THE COLE–COLE MODEL FOR A VISCOELASTIC MEDIUM

The numerical algorithm of the paper is based on the equations of conservation of momentum as well as the constitutive relations for an isotropic linear viscoelastic medium with singular memory, which undergoes relaxation according to the Cole–Cole law.

For two spatial dimensions, the equations of momentum conservation are of the following form (Fung 1965)

$$\dot{v}_x = \frac{1}{\rho}\frac{\partial \sigma_{xx}}{\partial x} + \frac{1}{\rho}\frac{\partial \sigma_{xz}}{\partial z} + \frac{f_x}{\rho}, \tag{1a}$$

$$\dot{v}_z = \frac{1}{\rho}\frac{\partial \sigma_{xz}}{\partial x} + \frac{1}{\rho}\frac{\partial \sigma_{zz}}{\partial z} + \frac{f_z}{\rho}, \tag{1b}$$

where x and z are the horizontal and vertical coordinates respectively, v_x, v_z are the horizontal and vertical velocity components, σ_{xx}, σ_{xz}, σ_{zz} are the stress components, f_x, f_z are body forces per unit volume, ρ denotes the density of the heterogeneous viscoelastic medium and a dot above a variable represents a derivative with respect to time.

The stress–strain constitutive relation of the Cole–Cole model is determined by the complex modulus (Cole & Cole 1941)

$$M(\omega) = M_\infty \frac{1 + a(i\eta\omega)^{-\alpha}}{1 + (i\eta\omega)^{-\alpha}} = M_\infty + \frac{M_\infty(a-1)}{1 + (i\eta\omega)^{\alpha}},$$
$$a = \frac{M_0}{M_\infty}, \quad 0 < \alpha < 1, a \le 1, \tag{2}$$

where $M(\omega)$ is the frequency-dependent complex modulus, M_∞ is the limit of the complex modulus for $\omega \to \infty$, M_0 is the value of the complex modulus for $\omega = 0$, η is a characteristic relaxation time and α controls the width of the transition zone between M_∞ and M_0. Besides, the conditions $0 < \alpha < 1$ and $a \le 1$ follow from thermodynamics argument (Bagley & Torvik 1983).

The stress relaxation function $\psi(t)$ and the derivative of the stress relaxation function $\psi_{,t}(t)$ for the Cole–Cole law have the following expressions (Hanyga 2003a)

$$\psi(t) = M_\infty \left\{ a + (1-a) E_\alpha \left[-\left(\frac{t}{\eta}\right)^\alpha \right] \right\} H(t), \tag{3a}$$

$$\psi_{,t}(t) = M_\infty \left\{ \delta(t) + \frac{1-a}{\eta}\left(\frac{t}{\eta}\right)^{\alpha-1} E_{\alpha,\alpha}\left[-\left(\frac{t}{\eta}\right)^\alpha \right] \right\}, \tag{3b}$$

where $H(t)$ is the Heaviside function and $E_{\gamma,\beta}(z)$ denotes the generalized Mittag–Leffler function (Podlubny 1998)

$$E_{\gamma,\beta}(z) := \sum_{n=0}^{\infty} \frac{z^n}{\Gamma(\gamma n + \beta)} \tag{4}$$

and $E_\gamma(z) := E_{\gamma,1}(z)$. The stress of a 1-D viscoelastic medium

characterized by the Cole–Cole law can be represented by the convolution of the derivative of stress relaxation function $\psi_{,t}(t)$ and strain $\varepsilon(t)$ (Christensen 1971):

$$\sigma(t) = \psi_{,t}(t) * \varepsilon(t) \tag{5}$$

where $*$ denotes the convolution operator. It follows from eq. (3b) that the second term in the kernel $\psi_{,t}(t)$ in eq. (5) is weakly singular for $t \to 0$.

The constitutive relation for a 1-D viscoelastic medium has the following form in the frequency domain:

$$\tilde{\sigma}(\omega) = M(\omega)\tilde{\varepsilon}(\omega), \tag{6}$$

where $\tilde{\sigma}(\omega)$, $\tilde{\varepsilon}(\omega)$ denote the Fourier transform of stress and strain, $M(\omega)$ denote the frequency-dependent complex modulus as shown in eq. (2) and $M(\omega) = F(\psi_{,t}(t))$, the symbol F represents the Fourier transformation and a tilde over a variable denotes the Fourier transform of the original variable.

In a linear isotropic viscoelastic medium with singular memory, the *P*- and *S*-wave modes satisfy the Cole–Cole relaxation law with different parameters. Consequently, in terms of the Cole–Cole models for *P* and *S* waves, one has

$$\begin{aligned}\tilde{\lambda}(\omega) + 2\tilde{\mu}(\omega) &= M_{\infty p}\frac{1 + a_p(i\eta_p\omega)^{-\alpha_p}}{1 + (i\eta_p\omega)^{-\alpha_p}} \\ &= M_{\infty p} + \frac{M_{\infty p}(a_p - 1)}{1 + (i\eta_p\omega)^{\alpha_p}},\end{aligned} \tag{7a}$$

$$\tilde{\mu}(\omega) = M_{\infty s}\frac{1 + a_s(i\eta_s\omega)^{-\alpha_s}}{1 + (i\eta_s\omega)^{-\alpha_s}} = M_{\infty s} + \frac{M_{\infty s}(a_s - 1)}{1 + (i\eta_s\omega)^{\alpha_s}}, \tag{7b}$$

where the subscript p, s denote the *P* and *S* waves in a viscoelastic medium and $\tilde{\lambda}(\omega)$, $\tilde{\mu}(\omega)$ are the complex modulus corresponding to the two Lame constants. The frequency-domain constitutive relations for a 2-D Cole–Cole viscoelastic medium are as follows

$$\begin{aligned}\tilde{\sigma}_{xx}(\omega) = {} & M_{\infty p}\tilde{v}_{x,x}(\omega) + M_{\infty p}\tilde{v}_{z,z}(\omega) - 2M_{\infty s}\tilde{v}_{z,z}(\omega) \\ & + \frac{M_{\infty p}(a_p - 1)}{1 + (i\eta_p\omega)^{\alpha_p}}[\tilde{v}_{x,x}(\omega) + \tilde{v}_{z,z}(\omega)] \\ & - 2\frac{M_{\infty s}(a_s - 1)}{1 + (i\eta_s\omega)^{\alpha_s}}\tilde{v}_{z,z}(\omega),\end{aligned} \tag{8a}$$

$$\begin{aligned}\tilde{\sigma}_{zz}(\omega) = {} & M_{\infty p}\tilde{v}_{x,x}(\omega) + M_{\infty p}\tilde{v}_{z,z}(\omega) - 2M_{\infty s}\tilde{v}_{x,x}(\omega) \\ & + \frac{M_{\infty p}(a_p - 1)}{1 + (i\eta_p\omega)^{\alpha_p}}[\tilde{v}_{x,x}(\omega) + \tilde{v}_{z,z}(\omega)] \\ & - 2\frac{M_{\infty s}(a_s - 1)}{1 + (i\eta_s\omega)^{\alpha_s}}\tilde{v}_{x,x}(\omega),\end{aligned} \tag{8b}$$

$$\begin{aligned}\tilde{\sigma}_{zx}(\omega) = {} & M_{\infty s}\tilde{v}_{x,z}(\omega) + M_{\infty s}\tilde{v}_{z,x}(\omega) \\ & + \frac{M_{\infty s}(a_s - 1)}{1 + (i\eta_s\omega)^{\alpha_s}}[\tilde{v}_{x,z}(\omega) + \tilde{v}_{z,x}(\omega)].\end{aligned} \tag{8c}$$

The constitutive relations for the viscoelastic medium in the frequency domain can be rewritten in terms of internal variables $\tilde{\chi}^p_{zx}(\omega)$, $\tilde{\chi}^s_{xx}(\omega)$, $\tilde{\chi}^s_{zz}(\omega)$, $\tilde{\chi}^s_{zx}(\omega)$ (Hanyga 2003b):

$$\begin{aligned}\tilde{\sigma}_{xx}(\omega) = {} & M_{\infty p}\tilde{v}_{x,x}(\omega) + M_{\infty p}\tilde{v}_{z,z}(\omega) \\ & - 2M_{\infty s}\tilde{v}_{z,z}(\omega) + \tilde{\chi}^p_{zx}(\omega) - 2\tilde{\chi}^s_{zz}(\omega),\end{aligned} \tag{9a}$$

$$\begin{aligned}\tilde{\sigma}_{zz}(\omega) = {} & M_{\infty p}\tilde{v}_{x,x}(\omega) + M_{\infty p}\tilde{v}_{z,z}(\omega) \\ & - 2M_{\infty s}\tilde{v}_{x,x}(\omega) + \tilde{\chi}^p_{zx}(\omega) - 2\tilde{\chi}^s_{xx}(\omega),\end{aligned} \tag{9b}$$

$$\tilde{\sigma}_{zx}(\omega) = M_{\infty s}\tilde{v}_{x,z}(\omega) + M_{\infty s}\tilde{v}_{z,x}(\omega) + \tilde{\chi}^s_{zx}(\omega). \tag{9c}$$

The Fourier transforms of the internal variables $\tilde{\chi}^p_{zx}(\omega)$, $\tilde{\chi}^s_{xx}$, $\tilde{\chi}^s_{zz}(\omega)$, $\tilde{\chi}^s_{zx}(\omega)$ are given by the expressions

$$\tilde{\chi}^p_{zx}(\omega) = \frac{M_{\infty p}(a_p - 1)}{1 + (i\eta_p\omega)^{\alpha_p}}[\tilde{v}_{x,x}(\omega) + \tilde{v}_{z,z}(\omega)], \tag{10a}$$

$$\tilde{\chi}^s_{xx}(\omega) = \frac{M_{\infty s}(a_s - 1)}{1 + (i\eta_s\omega)^{\alpha_s}}\tilde{v}_{x,x}(\omega), \tag{10b}$$

$$\tilde{\chi}^s_{zz}(\omega) = \frac{M_{\infty s}(a_s - 1)}{1 + (i\eta_s\omega)^{\alpha_s}}\tilde{v}_{z,z}(\omega), \tag{10c}$$

$$\tilde{\chi}^s_{zx}(\omega) = \frac{M_{\infty s}(a_s - 1)}{1 + (i\eta_s\omega)^{\alpha_s}}[\tilde{v}_{x,z}(\omega) + \tilde{v}_{z,x}(\omega)]. \tag{10d}$$

The inverse Fourier transformation of eqs (9) and (10)) yields following equations

$$\begin{aligned}\dot{\sigma}_{xx}(t) = {} & M_{\infty p}v_{x,x}(t) + M_{\infty p}v_{z,z}(t) \\ & - 2M_{\infty s}v_{z,z}(t) + \chi^p_{zx}(t) - 2\chi^s_{zz}(t),\ \sigma_{xx}(0) = 0,\end{aligned} \tag{11a}$$

$$\begin{aligned}\dot{\sigma}_{zz}(t) = {} & M_{\infty p}v_{x,x}(t) + M_{\infty p}v_{z,z}(t) \\ & - 2M_{\infty s}v_{x,x}(t) + \chi^p_{zx}(t) - 2\chi^s_{xx}(t),\ \sigma_{zz}(0) = 0,\end{aligned} \tag{11b}$$

$$\dot{\sigma}_{zx}(t) = M_{\infty s}v_{x,z}(t) + M_{\infty s}v_{z,x}(t) + \chi^s_{zx}(t),\ \sigma_{zx}(0) = 0, \tag{11c}$$

$$\begin{aligned}D^{\alpha_p}\chi^p_{zx}(t) = {} & -\frac{1}{\eta_p^{\alpha_p}}\chi^p_{zx}(t) + \frac{M_{\infty p}(a_p - 1)}{\eta_p^{\alpha_p}}[v_{x,x}(t) + v_{z,z}(t)], \\ & \chi^p_{zx}(0) = 0,\end{aligned} \tag{11d}$$

$$D^{\alpha_s}\chi^s_{xx}(t) = -\frac{1}{\eta_s^{\alpha_s}}\chi^s_{xx}(t) + \frac{M_{\infty s}(a_s - 1)}{\eta_s^{\alpha_s}}v_{x,x}(t), \quad \chi^s_{xx}(0) = 0, \tag{11e}$$

$$D^{\alpha_s}\chi^s_{zz}(t) = -\frac{1}{\eta_s^{\alpha_s}}\chi^s_{zz}(t) + \frac{M_{\infty s}(a_s - 1)}{\eta_s^{\alpha_s}}v_{z,z}(t), \quad \chi^s_{zz}(0) = 0, \tag{11f}$$

$$\begin{aligned}D^{\alpha_s}\chi^s_{zx}(t) = {} & -\frac{1}{\eta_s^{\alpha_s}}\chi^s_{zx}(t) + \frac{M_{\infty s}(a_s - 1)}{\eta_s^{\alpha_s}}[v_{x,z}(t) + v_{z,x}(t)], \\ & \chi^s_{zx}(0) = 0,\end{aligned} \tag{11g}$$

where D^α denotes the Caputo fractional derivative of α order with zero as the lower terminal (Podlubny 1998).

For the present 2-D viscoelastic problem, the equations can be formulated in terms of velocities $v_x(t)$, $v_z(t)$ and stresses $\sigma_{xx}(t)$, $\sigma_{zz}(t)$, $\sigma_{zx}(t)$ and the four internal variables $\chi^p_{zx}(t)$, $\chi^s_{xx}(t)$, $\chi^s_{zz}(t)$, $\chi^s_{zx}(t)$, which are related to the velocity by the fractional differential eqs (11d–g). Eq. (1) together with eq. (11) provide all the equations needed to determine the velocities, the stresses and the four internal variables.

3 A NEW METHOD FOR SOLVING OF FRACTIONAL DIFFERENTIAL EQUATIONS OF $D^\alpha\chi(t) = f[\chi(t), t]$ TYPE

Before proceeding to solve the viscoelastic system, we shall discuss the fractional differential equation

$$D^\alpha\chi(t) = f[\chi(t), t], \tag{12a}$$

$$\chi(0) = 0. \tag{12b}$$

Several numerical methods have been proposed for integration of the fractional differential equation of eq. (12) (Gorenflo & Mainardi 1997; Diethelm *et al.* 2002). Mechanical damping involving a fractional derivative for a distributed system is studied by Padovan (1987) and Enelund & Olsson (1999). These models are based on the Finite Element Method (FEM) discretization. The main drawback of these methods is the necessity of storing and integrating the entire history of $\chi(t)$. As a result, a numerical scheme combining the above methods with the PS method for an unbounded medium is excessively expensive. Recently, Yuan & Agrawal (2002) proposed a new numerical approach, which does not require integration and storage of all the history of the variables to be evaluated. However, unfortunately, as will be demonstrated below, the Yuan and Agrawal method, which was originally applied to discrete mechanical systems is not satisfactorily accurate for viscoelastic boundary-value problems. Hence, in this section, an improvement of the Yuan and Agrawal method for solving the fractional differential equation will be made.

The key point of Yuan and Agrawal's method is to transform the fractional derivative into an infinite integral and use a specific quadrature formula to evaluate the infinite integral. In this way, the fractional derivative can be evaluated by a series of quadrature variables satisfying first-order ordinary differential equations. Following Yuan & Agrawal (2002), the Caputo fractional derivative of order α, $0 < \alpha < 1$ with zero as the lower terminal can be evaluated by the following expressions:

$$D^{\alpha}\chi(t) = \frac{2\sin(\pi\alpha)}{\pi}\int_0^{+\infty}\phi(y,t)\,dy, \tag{13a}$$

$$\phi(y,t) = y^{2\alpha-1}\int_0^t e^{-(t-\tau)y^2}D\chi(\tau)\,d\tau, \tag{13b}$$

$$\dot{\phi}(y,t) = -y^2\phi(y,t) + y^{2\alpha-1}D\chi(t), \tag{13c}$$

where $D := d/dt$. Using the Laguerre quadrature formula (Davis & Rabinowitz 1984) to approximate the infinite integral in eq. (13a), the fractional differential eq. (12a) is approximated by the equations

$$\kappa\sum_{i=1}^{N} w_i^{(N)} e^{y_i^{(N)}}\phi\big[y_i^{(N)},t\big] = f[\chi(t),t], \tag{14a}$$

$$\dot{\phi}\big[y_i^{(N)},t\big] = -y_i^{(N)^2}\phi\big[y_i^{(N)},t\big] + y_i^{(N)^{2\alpha-1}}D\chi(t), \tag{14b}$$

where N denotes the number of the quadrature points used in the Laguerre quadrature formula, $y_i^{(N)}$, $w_i^{(N)}$, $i = 1, \ldots, N$ are the quadrature points and corresponding weights in the Laguerre quadrature formula and $\kappa = 2\sin(\pi\alpha)/\pi$. Differentiation of eq. (14a) and substitution of eq. (14b) yield the first-order ordinary differential equation for $\chi(t)$. The solutions of $\chi(t)$ and $\phi(y_i^{(N)},t), i = 1, \ldots, N$ can be determined by the numerical solution of the first-order ordinary differential equation of $\chi(t)$ along with those of $\phi(y_i^{(N)},t)$, $i = 1, \ldots, N$ given by eq. (14b).

We begin with a numerical test of the approximation eq. (14) applied to eq. (11d) with $v_{x,x}(t) + v_{z,z}(t)$ given by the Ricker wavelet (Ricker 1977)

$$R(t) = \left[\frac{\omega_c(t-t_s)^2}{2} - 1\right]e^{[-\omega_c(t-t_s)^2/4]}. \tag{15}$$

Therefore, eq. (11d) is recast in the form

$$D^{\alpha_p}\chi_{zx}^{p}(t) = -\frac{1}{\eta_p^{\alpha_p}}\chi_{zx}^{p}(t) + \frac{M_{\infty p}(a_p-1)}{\eta_p^{\alpha_p}}R(t). \tag{16}$$

The numerical approximation of $\chi_{zx}^{p}(t)$ constructed by applying eq. (14) to eq. (16) is compared with the solutions calculated by the Fast Fourier transformation (FFT) of the frequency domain eq. (10a). For numerical demonstration we assume the following parameters of the medium: $M_{\infty p} = 8.0 \times 10^9$ Pa, $\eta_p = 2.0 \times 10^{-2}$ s, $a_p = 0.5$, $\alpha_p = 0.5$, 0.7, 0.9 respectively. The Ricker wavelet parameters ω_c, t_s in eq. (15) are taken as 400π s^{-1} and 0.02 s respectively. The number N of quadrature points in eq. (14) is 35. The variable $\chi_{zx}^{p}(t)$ calculated by the method of eq. (14) and by the FFT method is shown in Fig. 1. It follows from Fig. 1 that there are significant differences between the two solutions. Moreover, the differences between the two solutions become more pronounced when α_p assumes larger values.

The reason for this shortcoming is the singularity of the Cole–Cole kernel and slow convergence of the quadrature formula at zero and infinity. The convergence can be improved by using a more accurate quadrature formula to evaluate the infinite integral of eq. (13a). It is easy to get the following asymptotic expression of $\phi(y,t)$ for $y \to 0$:

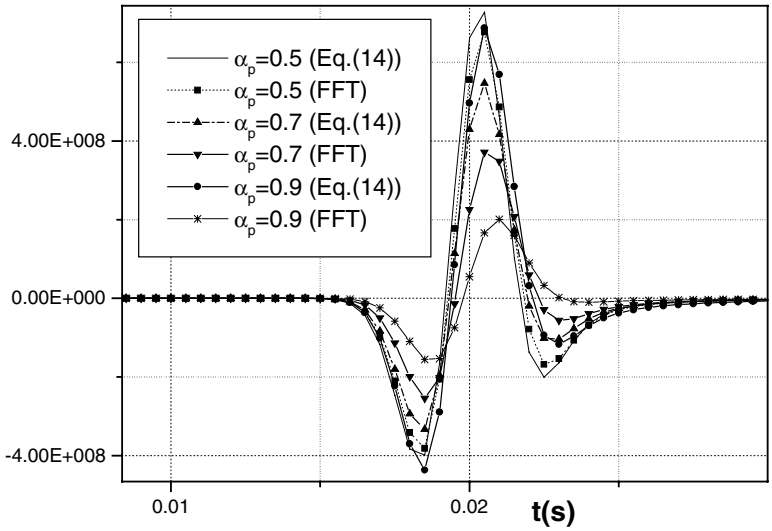

Figure 1. Comparison between the solutions of the fractional differential equation by the Yuan–Agrawal method and the FFT method.

$$\phi(y,t) \approx y^{2\alpha-1}\int_0^t D\chi(\tau)\,d\tau. \tag{17}$$

If the initial condition eq. (12b) is adopted, then

$$\phi(y,t) \approx y^{2\alpha-1}\chi(t). \tag{18}$$

On the other hand, if one assumes that $\chi(t)$ has a second-order derivative, then integration of eq. (13b) by part yields the following equation:

$$\phi(y,t) = y^{2\alpha-1}\left\{\left[\frac{1}{y^2}e^{-(t-\tau)y^2}D\chi(\tau)\right]\Big|_0^t - \frac{1}{y^2}\int_0^t e^{-(t-\tau)y^2}D^2\chi(\tau)\,d\tau\right\}. \tag{19}$$

In terms of the above equation, the asymptotic expression for $\phi(y, t)$ when y tends to infinity can be written as

$$\phi(y,t) \approx y^{2\alpha-3}D\chi(t). \tag{20}$$

In terms of eqs (18) and (20), one can conclude that when α tends to zero or one, the infinite integral in eq. (13a) will converge very slowly. Consequently, in this case, it is difficult to use the above mentioned Laguerre integral formula to evaluate the infinite integral.

In order to accelerate the convergence of the infinite integral, eq. (13a) can be rewritten in the following form:

$$\begin{aligned} D^\alpha\chi(t) &= \kappa\int_0^{+\infty}\phi(y,t)\,dy = \kappa\int_0^c[\phi(y,t)-y^{2\alpha-1}\chi(t)]\,dy \\ &\quad+\kappa\int_c^{+\infty}[\phi(y,t)-y^{2\alpha-3}D\chi(t)]\,dy \\ &\quad+\kappa\int_0^c y^{2\alpha-1}\chi(t)\,dy+\kappa\int_c^{+\infty}y^{2\alpha-3}D\chi(t)\,dy, \end{aligned} \tag{21}$$

where c is a constant. The first two integrals in the above equation converge much faster than the original one, while the second two integrals can be evaluated in closed form. Evaluating the first two integrals by the Gauss and shifted Laguerre quadrature formulae (Davis & Rabinowitz 1984), one has

$$\begin{aligned} D^\alpha\chi(t) &= \kappa\sum_{i=1}^{n_G}w_i^G\phi\left(y_i^G,t\right)+\kappa\sum_{i=1}^{n_L}w_i^L\phi\left(y_i^L,t\right) \\ &\quad+\Psi_G\chi(t)+\Psi_L D\chi(t), \end{aligned} \tag{22}$$

where n_G, n_L are the number of quadrature points for the Gauss quadrature formula and the shifted Laguerre integral formula respectively, $y_i^G (i = 1, 2, \ldots, n_G)$ and $y_i^L (i = 1, 2, \ldots, n_L)$ are the abscissas for the quadrature points of the Gauss formula and the shifted Laguerre integral formula respectively, $w_i^G (i = 1, 2, \ldots, n_G)$ and $w_i^L (i = 1, 2, \ldots, n_L)$ are the corresponding quadrature weights. In addition, Ψ_G, Ψ_L are given by

$$\Psi_G = \kappa\left[\frac{c^{2\alpha}}{2\alpha}-\sum_{i=1}^{n_G}w_i^G\left(y_i^G\right)^{2\alpha-1}\right],$$

$$\Psi_L = \kappa\left[\frac{c^{2\alpha-2}}{2-2\alpha}-\sum_{i=1}^{n_L}w_i^L\left(y_i^L\right)^{2\alpha-3}\right]. \tag{23a,b}$$

Combination of the first two terms in eq. (22) yields

$$D^\alpha\chi(t) = \kappa\sum_{i=1}^{N_I}w_i\phi(y_i,t)+\Psi_G\chi(t)+\Psi_L D\chi(t), \tag{24a}$$

$$w_i = \begin{cases} w_i^G, i \le n_G \\ w_{i-n_G}^L, i > n_G \end{cases}, \quad i = 1, 2, \ldots, N_I,$$

$$y_i = \begin{cases} y_i^G, i \le n_G \\ y_{i-n_G}^L, i > n_G \end{cases}, = 1, 2, \ldots, N_I, \tag{24b,c}$$

where $N_I = n_G + n_L$. The above regularization of the integral (13a) accelerates its convergence and accounts for the singularity at $y = 0$ and $y = \infty$. Substituting eq. (24a) into eq. (12a) and combining it with eq. (14b) yields

$$\dot\chi(t) = -\frac{\kappa}{\Psi_L}\sum_{i=1}^{N_I}w_i\phi(y_i,t)-\frac{\Psi_G}{\Psi_L}\chi(t)+\frac{1}{\Psi_L}f[\chi(t),t], \tag{25a}$$

$$\dot\phi(y_i,t) = -y_i^2\phi(y_i,t)+y_i^{2\alpha-1}\left\{-\frac{\kappa}{\Psi_L}\sum_{i=1}^{N_I}w_i\phi(y_i,t) - \frac{\Psi_G}{\Psi_L}\chi(t)+\frac{1}{\Psi_L}f[\chi(t),t]\right\}, i = 1, 2, \ldots, N_I, \tag{25b}$$

$$\chi(0) = 0, \phi(y_i, 0) = 0, i = 1, 2, \ldots, N_I. \tag{25c,d}$$

The fractional differential equation eq. (12) has been reduced to a system of ordinary differential equations in eq. (25) for the primary internal variable $\chi(t)$ and the secondary internal variables $\phi(y_i, t)$, $i = 1, 2, \ldots, N_I$. Using eq. (25) and the same parameters as above, eq. (16) is solved again. In calculation, $\alpha_p = 0.1, 0.5, 0.7, 0.9$, $n_G = 10$, $n_L = 25$ and $c = 1.0$. Again, the numerical results obtained by eq. (25) are compared with the results obtained by the FFT method. Fig. 2 shows clearly that the results obtained by the two approaches agree with each other very well.

The new method of solving the fractional differential eq. (12) has following advantages. In the first place, for the evaluation of the present solution, the storage and integration of the entire histories of internal variables are not needed. Furthermore, the method yields sufficiently accurate results for a fractional relaxation equation of a fractional order $0 < \alpha < 1$ by using a relatively small number of quadrature points, which is crucial for reducing the computational cost of the scheme to an acceptable level.

4 NUMERICAL SCHEME FOR THE COLE–COLE VISCOELASTIC MEDIUM

As pointed out above, the viscoelastic medium with singular memory is described by the eqs (1) and (11) together with the corresponding boundary conditions and the initial conditions. For the four fractional differential equations involved in eq. (11), the method developed in the last section will be applied. In this way, the four fractional differential equations can be reduced to a system of first-order ordinary differential equations for the primary and secondary internal variables. The first-order ordinary differential equations for the primary and secondary internal variables together with the equations for the velocity and stress constitute the system equations for the viscoelastic medium. The Fourier and Chebychev collocation methods used to calculate horizontal and vertical derivatives will be discussed in this section. Moreover, for the Chebychev PS method, the implementation of boundary conditions and non-reflecting conditions for the viscoelastic medium is analysed.

4.1 Equations in the matrix form

Combining eq. (25) with eq. (11) and using eq. (1), the differential equations for all the variables can be written in following matrix

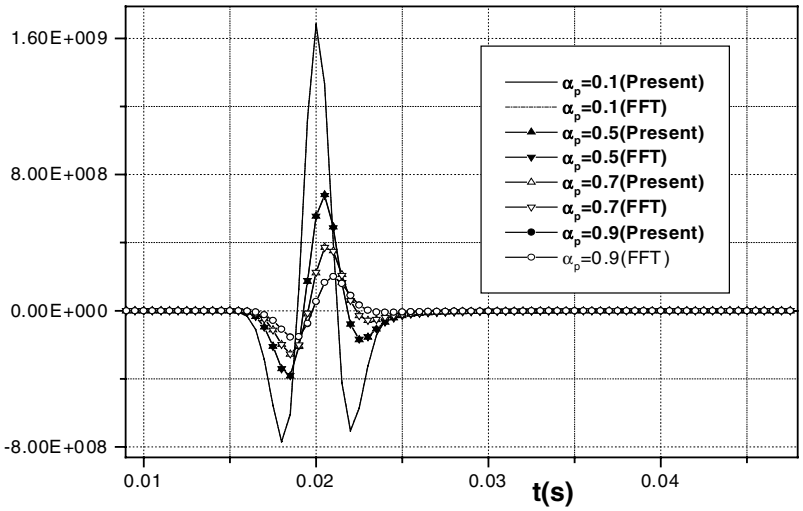

Figure 2. Comparison of the solutions of the fractional differential equation by the present method and the FFT method.

form:

$$\frac{\partial \mathbf{V}}{\partial t} = \mathbf{A}\frac{\partial \mathbf{V}}{\partial x} + \mathbf{B}\frac{\partial \mathbf{V}}{\partial z} + \mathbf{C}, \quad \mathbf{V}(0) = \mathbf{0}, \tag{26a,b}$$

where the unknown vector **V**, vector **C** and matrix **A**, **B** are given in the Appendix.

4.2 Fourier and Chebychev collocation methods

The horizontal coordinate x is discretized by the Fourier expansion and the derivatives are calculated by the fast Fourier transform (FFT) method. For the vertical derivative, the Chebychev PS method is employed, which facilitates the implementation of a free surface boundary condition. Moreover, for the Chebychev PS method, the spatial derivative is calculated by a modified FFT method.

In this paper, the Discrete Fourier transform (DFT) and Inverse Discrete Fourier transform (IDFT) are defined as follows (Oppenheim & Schafer 1999):

$$H_n := \sum_{k=0}^{N-1} h_k e^{-2\pi i k n/N}, \quad h_k := \frac{1}{N}\sum_{n=0}^{N-1} H_n e^{2\pi i k n/N}, \tag{27a,b}$$

where h_k, $k = 0, 1, 2, \ldots, N-1$, and H_n , $n = 0, 1, 2, \ldots, N-1$, are the N sample values in the spatial domain and in the transformed domain, respectively.

In the horizontal direction, the coordinates of the sampling points are given by:

$$x_k = \Delta x(k-1), \quad k = 1, 2, \ldots, N_x; \quad \Delta x = \frac{x_{\max}}{N_x - 1}, \tag{28a,b}$$

where $x_{\max}$ is the maximum distance in the horizontal direction, N_x is the number of the gridpoints in the horizontal direction and Δx is the mesh size. Note that the period of FFT in the horizontal direction is equal to $x_{\max} + \Delta x$. Moreover, as a result of the Hermitian property of the derivative, the N_x in the above equation should be an odd number (Carcione 2001). Obviously, if N_x is even, the DFT as shown in eq. (27) has a Nyquist component, which makes the corresponding derivative not have the Hermitian property. In terms of the definition of DFT in eq. (27), for a given function $f(x)$ with the transformed function $\tilde{f}(k_x)$, the derivatives of $f(x)$ are calculated by:

$$\frac{\tilde{d}f}{dx} = ik_x\tilde{f}(k_x); \tag{29a}$$

$$k_x = (j-1)\Delta k_x, \quad j \le \frac{N_x+1}{2};$$

$$k_x = -(N_x - j + 1)\Delta k_x, \quad j > \frac{N_x+1}{2}; \tag{29b,c}$$

$$\Delta k_x = \frac{2\pi}{N_x \Delta x}, \quad j = 1, 2, \ldots, N_x; \tag{29d}$$

where $i = \sqrt{-1}$.

As a result of the periodicity of the DFT, the Fourier PS method applies only to periodic problems. It is therefore difficult to take into account the free surface boundary condition by the Fourier PS method. Consequently, the vertical coordinate will be discretized by the Chebychev PS method. When solving problems by an explicit time marching method, the usual Chebychev differential operator requires time steps of the order $O(1/N^2)$ (N is the number of gridpoints), which makes the wave simulation very expensive. In order to overcome this difficulty, a modified Chebychev PS method, which allows time steps of the order $O(1/N)$, is adopted in the paper (Kosloff & Tal-Ezer 1993).

For the Chebychev PS method, the field variable $u(\xi)$, $-1 \le \xi \le 1$, can be expanded into a Chebychev polynomials $T_n(\xi)$:

$$u(\xi_j) = \sum_{n=1}^{N-1} a_n T_n(\xi_j) + \frac{1}{2}[a_0 T_0(\xi_j) + a_N T_N(\xi_j)], \; j = 0, 1, \ldots, N, \tag{30a}$$

$$\xi_j = \cos(\pi j/N), \; j = 0, 1, \ldots, N, \tag{30b}$$

where ξ_j are the Gauss–Lobatto collocation points. The first-order derivative of the variable $u(\xi)$, $-1 \le \xi \le 1$ can be evaluated from the equation

$$\frac{\partial u(\xi_j)}{\partial \xi} = \sum_{n=1}^{N-1} b_n T_n(\xi_j) + \frac{1}{2}[b_0 T_0(\xi_j) + b_N T_N(\xi_j)], \quad j = 0, 1, \ldots, N, \tag{31a}$$

$$b_{n-1} = b_{n+1} + 2n a_n, \quad n = N, N-1, \ldots, 1, \tag{31b}$$

where $b_{N+1} = b_N = 0$ (Gottlieb & Orszag 1977). Assuming the collocation points at $\xi_j = \cos(\pi j/N)$, $j = 0, 1, \ldots, N$, eqs (30a) and (31a) can be reduced to

$$u(\xi_j) = \sum_{n=1}^{N-1} a_n \cos(\pi n j/N) + \frac{1}{2}\left[a_0 + (-1)^j a_N\right], \tag{32a}$$

$$\frac{\partial u(\xi_j)}{\partial \xi} = \sum_{n=0}^{N} b_n \cos(\pi n j/N) + \frac{1}{2}\left[b_0 + (-1)^j b_N\right]. \quad (32b)$$

The above equations constitute the discrete cosine Fourier transformation. Therefore, the coefficients a_n, $n = 1, 2, .., N$ in eq. (32a) can be evaluated from $u(\xi_j)$, $j = 1, 2, \ldots, N$ by the inverse cosine transformation

$$a_n = \frac{2}{N}\sum_{j=1}^{N-1} u(\xi_j)\cos(\pi n j/N) + \frac{1}{N}\left[u(\xi_0) + (-1)^n u\left(\xi_N\right)\right]. \quad (33)$$

After determining the coefficients $a_n, n = 1, 2, .., N$, the coefficients b_n, $n = 1, 2, .., N$ can be determined by the recursion method of eq. (31b). Having obtained the coefficients $b_n, n = 1, 2, .., N$, again, the first-order derivative of $u(\xi)$ can be calculated by the FFT method as shown in eq. (32b).

It follows from eq. (30b) that the collocation points ξ_j are unevenly spaced in the interval $-1 \le \xi \le 1$. As mentioned above, the concentration of Chebychev collocation points near the boundary requires time steps of the order $O(1/N^2)$, which makes wavefield simulation very time-consuming. This problem is resolved by a coordinate transformation method, which yields numerical grids that are suitable for the solution of specific boundary-value problems.

For example, in the Lamb problem a free surface boundary condition at $z = 0$ and a non-reflecting condition at $z = z_{\max}$ are assumed. An asymmetric stretching function is used to generate gridpoints dense enough to model the free surface boundary condition but coarse enough to satisfy the stability condition. For $z = z_{\max}$, the non-reflecting boundary condition is imposed and a coarser grid can be adopted. The following non-symmetric transform function can serve the above purpose: (Kosloff *et al.* 1990)

$$q(\xi) = -\frac{1}{\sqrt{|c|}}\arcsin\left(\frac{2c\xi + b}{\sqrt{b^2 - 4c}}\right), \quad (34)$$

where

$$b = 0.5\alpha^{-2}(\beta^{-2} - 1), \quad c = 0.5\alpha^{-2}(\beta^{-2} + 1) - 1, \quad (35a,b)$$

α, β are two parameters that need to be specified. It can be shown that

$$\frac{d\xi}{dq} = \sqrt{1 + b\xi + c\xi^2}. \quad (36)$$

It can be seen that the amount of grid stretching at $\xi = -1$ is $dq/d\xi = \alpha$ and the stretching at $\xi = 1$ is $dq/d\xi = \alpha\ \beta$. Other kinds of mapping function can be found in Kosloff & Tal-Ezer (1993).

Furthermore, the following coordinate transformation,

$$z_j = z_{\max}\left[\frac{q(\xi_j) - q(1)}{q(-1) - q(1)}\right], j = 1, 2, \ldots, N, \quad (37)$$

maps the segment $[1, -1]$ of ξ onto the segment $[0, z_{\max}]$ of z.

If a map function as shown in eq. (37) is used, then, the spatial derivative of $u(\xi)$ with respect to z in the physical domain can be evaluated by following formula:

$$\frac{\partial u}{\partial z} = \frac{\partial u}{\partial \xi}\frac{\partial \xi}{\partial z} = \left[\frac{q(-1) - q(1)}{z_{\max}}\right]\frac{d\xi}{dq}\frac{\partial u}{\partial \xi}, \quad (38)$$

where $d\xi/dq$ is determined by the map function such as eq. (34) and $\partial u/\partial \xi$ can be evaluated by the above mentioned FFT method.

4.3 Boundary conditions

The free surface boundary condition requires zero values for σ_{zx}, σ_{zz}on the surface $z = 0$. However, as was shown in Gottlieb *et al.* (1982) and Thompson (1990), a direct application of the free surface boundary condition without consideration of the other variables, such as v_x, v_z, σ_{xx} and the internal variables, leads to numerical instabilities. To overcome this difficulty, following Gottlieb *et al.* and Thompson, the differential equations are recast as a first-order hyperbolic system. Furthermore, the resulting first-order hyperbolic system is decomposed into wave modes describing outgoing and incoming waves at the boundary. Numerical stability can be achieved by requiring that outgoing wave modes are determined by the solution within the computational domain, while the incoming wave modes are determined by the boundary condition. Because the method is described by Gottlieb *et al.* (1982) and Thompson (1990), the details of the derivation of the boundary conditions will be omitted and only the resulting boundary conditions for basic variables, internal variables and quadrature variables will be presented.

Applying wave mode method to eq. (26a), the free surface boundary conditions for the velocities, stresses, primary and secondary internal variables for the grids at $z = 0$ are obtained as follows:

$$\dot{v}_x^{(n)} = \dot{v}_x^{(o)} + \frac{1}{\rho v_s}\dot{\sigma}_{zx}^{(o)}, \quad (39a)$$

$$\dot{v}_z^{(n)} = \dot{v}_z^{(o)} + \frac{1}{\rho v_p}\dot{\sigma}_{zz}^{(o)}, \quad (39b)$$

$$\dot{\sigma}_{xx}^{(n)} = \dot{\sigma}_{xx}^{(o)} - \frac{M_{\infty p} - 2M_{\infty s}}{M_{\infty p}}\dot{\sigma}_{zz}^{(o)}, \quad (39c)$$

$$\dot{\sigma}_{zz}^{(n)} = 0, \quad (39d)$$

$$\dot{\sigma}_{zx}^{(n)} = 0, \quad (39e)$$

$$\dot{\chi}_{zx}^{p(n)} = \dot{\chi}_{zx}^{p(o)} - \frac{\delta_p}{M_{\infty p}}\dot{\sigma}_{zz}^{(o)}, \quad (39f)$$

$$\dot{\chi}_{xx}^{s(n)} = \dot{\chi}_{xx}^{s(o)}, \quad (39g)$$

$$\dot{\chi}_{zz}^{s(n)} = \dot{\chi}_{zz}^{s(o)} - \frac{\delta_s}{M_{\infty p}}\dot{\sigma}_{zz}^{(o)}, \quad (39h)$$

$$\dot{\chi}_{zx}^{s(n)} = \dot{\chi}_{zx}^{s(o)} - \frac{\delta_s}{M_{\infty s}}\dot{\sigma}_{zx}^{(o)}, \quad (39i)$$

$$\dot{\phi}_{zx_i}^{p(n)} = \dot{\phi}_{zx_i}^{p(o)} - \frac{\delta_p y_{p_i}^{2\alpha_p - 1}}{M_{\infty p}}\dot{\sigma}_{zz}^{(o)}, \quad i = 1, 2, \ldots, N_I^p, \quad (39j)$$

$$\dot{\phi}_{xx_i}^{s(n)} = \dot{\phi}_{xx_i}^{s(o)}, \quad i = 1, 2, \ldots, N_I^s, \quad (39k)$$

$$\dot{\phi}_{zz_i}^{s(n)} = \dot{\phi}_{zz_i}^{s(o)} - \frac{\delta_s y_{s_i}^{2\alpha_s - 1}}{M_{\infty p}}\dot{\sigma}_{zz}^{(o)}, \quad i = 1, 2, \ldots, N_I^s, \quad (39l)$$

$$\dot{\phi}_{zx_i}^{s(n)} = \dot{\phi}_{zx_i}^{s(o)} - \frac{\delta_s y_{s_i}^{2\alpha_s - 1}}{M_{\infty s}}\dot{\sigma}_{zx}^{(o)}, \quad i = 1, 2, \ldots, N_I^s, \quad (39m)$$

where $v_p = \sqrt{M_{\infty p}/\rho}$, $v_s = \sqrt{M_{\infty s}/\rho}$, the meanings of δ_p, δ_s, N_p^I, N_I^s, y_{p_i} and y_{s_i} are given in the Appendix and the superscript (o) denotes the time derivatives evaluated directly by the right-hand side of eq. (26a) at each time step, while (n) denotes the modified time derivatives resulting from the application of the free surface boundary condition. Note that when the time derivatives are used

to calculate the variable vector at each time step, the modified time derivatives are used.

Similarly, the non-reflecting radiation conditions at $z = z_{\max}$ for the velocities, stresses, primary and secondary internal variables are obtained as follows:

$$\dot{v}_x^{(n)} = \frac{1}{2}\left[\dot{v}_x^{(o)} - \frac{1}{\rho v_s}\dot{\sigma}_{zx}^{(o)}\right], \tag{40a}$$

$$\dot{v}_z^{(n)} = \frac{1}{2}\left[\dot{v}_z^{(o)} - \frac{1}{\rho v_p}\dot{\sigma}_{zz}^{(o)}\right], \tag{40b}$$

$$\dot{\sigma}_{xx}^{(n)} = \dot{\sigma}_{xx}^{(o)} - \frac{M_{\infty p} - 2M_{\infty s}}{2M_{\infty p}}\left[\dot{\sigma}_{zz}^{(o)} + \rho v_p \dot{v}_z^{(o)}\right], \tag{40c}$$

$$\dot{\sigma}_{zz}^{(n)} = \frac{1}{2}\left[\dot{\sigma}_{zz}^{(o)} - \rho v_p \dot{v}_z^{(o)}\right], \tag{40d}$$

$$\dot{\sigma}_{zx}^{(n)} = \frac{1}{2}\left[\dot{\sigma}_{zx}^{(o)} - \rho v_s \dot{v}_x^{(o)}\right], \tag{40e}$$

$$\dot{\chi}_{zx}^{p(n)} = \dot{\chi}_{zx}^{p(o)} - \frac{\delta_p}{2M_{\infty p}}\left[\dot{\sigma}_{zz}^{(o)} + \rho v_p \dot{v}_z^{(o)}\right], \tag{40f}$$

$$\dot{\chi}_{xx}^{s(n)} = \dot{\chi}_{xx}^{s(o)}, \tag{40g}$$

$$\dot{\chi}_{zz}^{s(n)} = \dot{\chi}_{zz}^{s(o)} - \frac{\delta_s}{2M_{\infty p}}\left[\dot{\sigma}_{zz}^{(o)} + \rho v_p \dot{v}_z^{(o)}\right], \tag{40h}$$

$$\dot{\chi}_{zx}^{s(n)} = \dot{\chi}_{zx}^{s(o)} - \frac{\delta_s}{2M_{\infty s}}\left[\dot{\sigma}_{zx}^{(o)} + \rho v_s \dot{v}_x^{(o)}\right], \tag{40i}$$

$$\dot{\phi}_{zx_i}^{p(n)} = \dot{\phi}_{zx_i}^{p(o)} - \frac{\delta_p y_{p_i}^{2\alpha_p - 1}}{2M_{\infty p}}\left[\dot{\sigma}_{zz}^{(o)} + \rho v_p \dot{v}_z^{(o)}\right], i = 1, 2, \ldots, N_I^p, \tag{40j}$$

$$\dot{\phi}_{xx_i}^{s(n)} = \dot{\phi}_{xx_i}^{s(o)}, \quad i = 1, 2, \ldots, N_I^s, \tag{40k}$$

$$\dot{\phi}_{zz_i}^{s(n)} = \dot{\phi}_{zz_i}^{s(o)} - \frac{\delta_s y_{s_i}^{2\alpha_s - 1}}{2M_{\infty p}}\left[\dot{\sigma}_{zz}^{(o)} + \rho v_p \dot{v}_z^{(o)}\right], i = 1, 2, \ldots, N_I^s, \tag{40l}$$

$$\dot{\phi}_{zx_i}^{s(n)} = \dot{\phi}_{zx_i}^{s(o)} - \frac{\delta_s y_{s_i}^{2\alpha_s - 1}}{2M_{\infty s}}\left[\dot{\sigma}_{zx}^{(o)} + \rho v_s \dot{v}_x^{(o)}\right], i = 1, 2, \ldots, N_I^s. \tag{40m}$$

The above method reduces the reflections from the bottom of the grids ($z = z_{\max}$). However, it does not eliminate them completely, especially for the waves of non-vertical incidence angles. Therefore, an absorbing region is added along the bottom and the sides of the computational domain to prevent wraparound and boundary reflection (Kosloff & Kosloff 1986).

5 NUMERICAL RESULTS

In order to check the correctness of the presented method, the first example simulates Lamb's problem with singular memory characterized by the Cole–Cole law. Our results from the PS method are compared with the results obtained by the potential method. In the second example, the case of a homogeneous viscoelastic layer over a viscoelastic half-space is considered. In the third example, the wavefield of a viscoelastic medium with modulus increasing linearly with depth will be calculated.

5.1 Example A: the viscoelastic Lamb problem

In this example, the wave propagation in a homogenous viscoelastic half plane with singular memory is simulated. The relaxation model of the medium is represented by the Cole–Cole law. Our results from the PS method are compared with those from the analytical method. The analytical method is based on the potential method. To begin with, we analyse Lamb's problem (Fig. 3) in the frequency domain. In the frequency domain, the two potentials for a 2-D viscoelastic medium satisfy the following equations: (Achenbach 1973)

$$\nabla^2\varphi + k_p^2\varphi = 0, \quad \nabla^2\psi + k_s^2\psi = 0, \tag{41a,b}$$

where

$$k_p = \frac{\omega}{v_p}, \quad k_s = \frac{\omega}{v_s}, \quad v_p = \sqrt{\frac{M_p(\omega)}{\rho}}, \quad v_s = \sqrt{\frac{M_s(\omega)}{\rho}}. \tag{42a-d}$$

In order to solve the Lamb problem as shown in Fig. 3, the half plane is divided into two domains D_1 and D_2 above and below the source. The domains D_1 and D_2satisfy following surface boundary conditions and continuity conditions:

$$\begin{aligned}
&\sigma_{zx_1}(x, 0, t) = 0, \quad \sigma_{zz_1}(x, 0, t) = 0,\\
&u_{x_1}(x, h^-, t) = u_{x_2}(x, h^+, t),\\
&u_{z_1}(x, h^-, t) = u_{z_2}(x, h^+, t),\\
&\sigma_{zx_1}(x, h^-, t) = \sigma_{zx_2}(x, h^+, t),\\
&\sigma_{zz_2}(x, h^+, t) - \sigma_{zx_1}(x, h^-, t) = -\delta(x)R(t).
\end{aligned} \tag{43a-f}$$

Applying Fourier transform to variables x in eq. (41), the general solutions involving arbitrary constants are obtained. The frequency domain solutions are obtained by the numerical inversion of the Fourier transform. After determining the frequency domain solution, the time domain solutions are recovered by using the FFT method.

In this example, the parameters in the Cole–Cole law are as follows: $M_{\infty p} = 8.0 \times 10^9$ Pa, $M_{\infty s} = 3.38 \times 10^9$ Pa, $a_p = a_s = 0.75$, $\alpha_p = \alpha_s = 0.5$, $\eta_p = \eta_s = 1.0 \times 10^{-3}$ s and the density of the homogeneous viscoelastic medium is $\rho = 2.0 \times 10^3$ kg m^{-3}. Because the half plane is homogeneous, $n_{G_p} = n_{G_s} = 10$, $n_{L_p} = n_{L_s} = 15$ and $c_p = c_s = 1.0$ for all the gridpoints. A numerical grid $N_x \times N_z = 121 \times 121$ is used with the mapping function eq. (35)

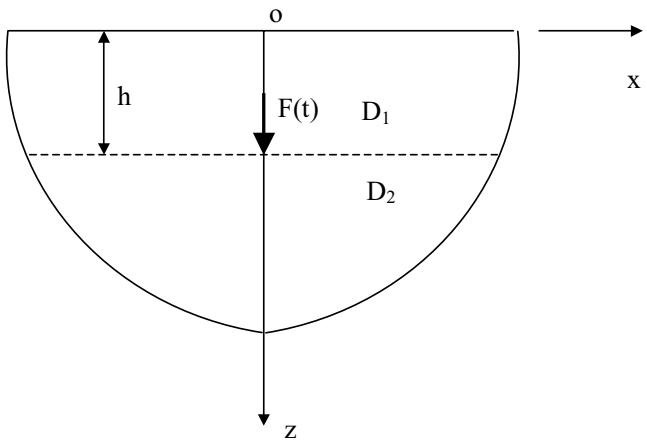

Figure 3. A half-plane viscoelastic medium subject to a point force.

for the z coordinate. The dimensions of the physical domain are $x_{\max} = 120$ m, $z_{\max} = 120$ m. The stretching parameters in eq. (35) are $\alpha = 9.86$, $\beta = 0.5$. The numerical grid has the free surface boundary condition at $z = 0$ and the non-reflecting condition for $z = z_{\max}$. As a result of the non-vertical incidence, the incoming waves cannot be completely eliminated. Therefore, absorbing strips of length 20 gridpoints are used at the two sides and lower boundary to prevent the residual non-physical reflection. The vertical force is of Ricker type as shown in eq. (15) and ω_c, t_s in eq. (15) are taken as 400π s^{-1} and 0.02 s, respectively. The force is applied at $x = 60$ m (gridpoint 61 of the horizontal direction) and at a depth of $z = 24.5299$ m (gridpoint 30 of the vertical direction). Two receiver points are located at $x = 30$ m, $z = 57.0652$ m (point 1) and $x = 40$ m, $z = 0.0$ m (point 2). The governing eq. (26a) is solved up to 0.1 s with a time step of 0.05 ms by using a second-order predictor–corrector method. A comparison of the results of the horizontal and vertical velocity for the two receivers from the PS method and the FFT method is shown in Fig. 4. It follows from Fig. 4 that the agreement between the PS method and the FFT method is quite good. A small error appears in the reflected waves as a result of the approximate treatment of the fractional derivative operator in our method.

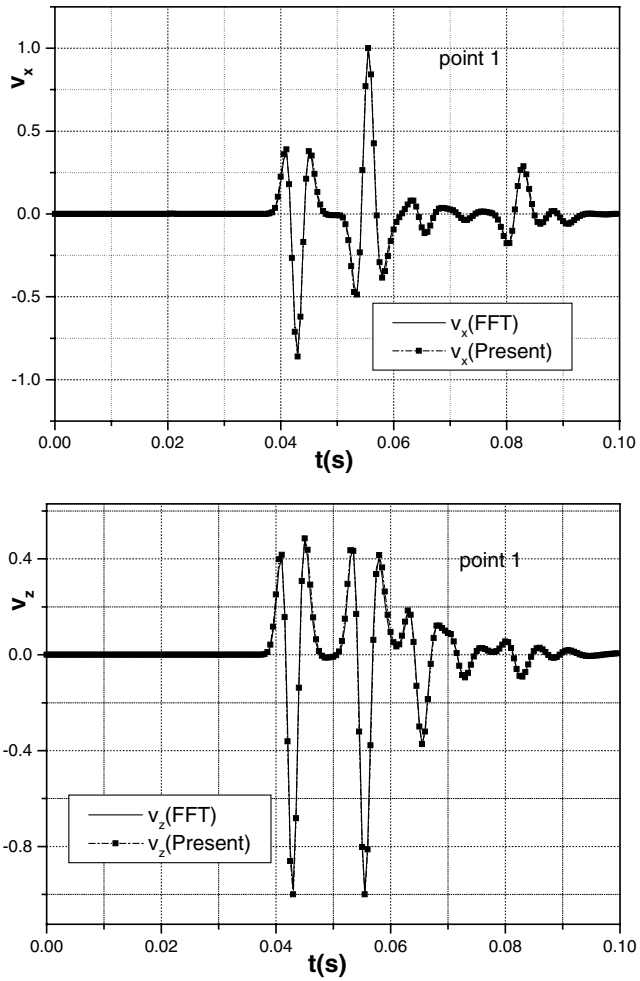

Figure 4. Comparison of the proposed method with the FFT method for the example A (Lamb problem): (a) v_x for point 1, (b) v_z for point 1, (c) v_x for point 2, (d) v_z for point 2.

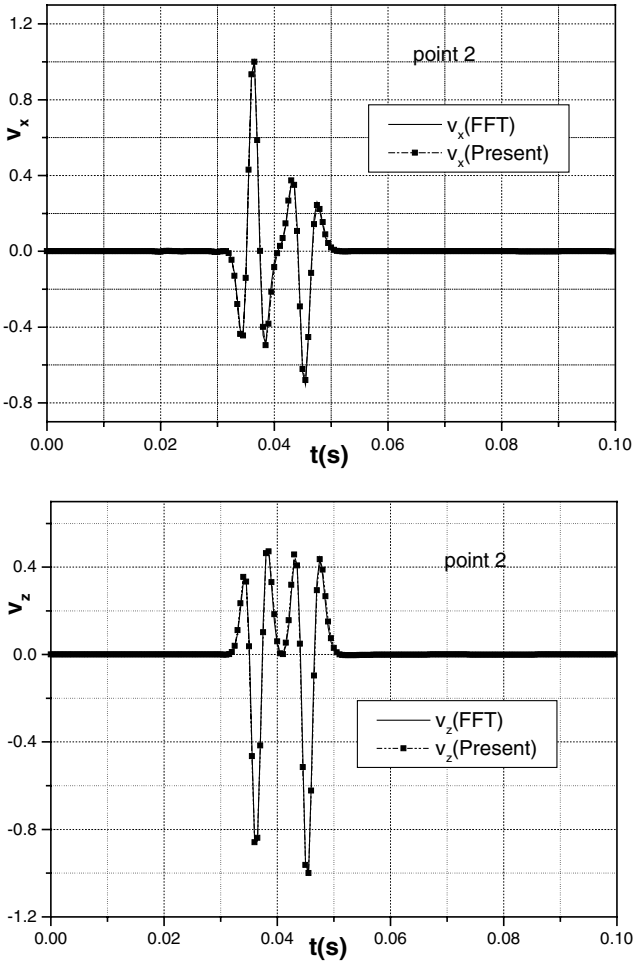

Figure 4. (*Continued.*)

5.2 Example B: a homogeneous viscoelastic layer over a viscoelastic half-space

In this example, the model consists of a homogeneous viscoelastic layer overlying a homogeneous half-space. The parameters of the layer are $M_{\infty p} = 6.0 \times 10^9$ Pa, $M_{\infty s} = 2.16 \times 10^9$ Pa, $\rho = 1500$ kg m^{-3}, $\eta_p = \eta_s = 0.1$ s, $a_p = a_s = 0.7$, $\alpha_p = \alpha_s = 0.7$, while the parameters for the half-space are $M_{\infty p} = 1.80 \times 10^{10}$ Pa, $M_{\infty s} = 5.12 \times 10^9$ Pa, $\rho = 2000$ kg m^{-3}, $\eta_p = \eta_s = 0.3$ s, $a_p = a_s = 0.8$, $\alpha_p = \alpha_s = 0.5$. The width and the depth of the calculation domain are 1000 and 600 m, respectively. The thickness of the layer is 300 m. In calculation, the grid size is 101 in the horizontal direction and 101 in the vertical direction. The numerical grid has a free surface boundary condition at $z = 0$ and a non-reflecting condition at $z = z_{\max}$. The absorbing strips of 20 grids are used laterally and at the bottom to eliminate the residual non-physical reflections. Because the horizontal interface has to be accounted for, the following transformation for the vertical coordinate is applied (Augenbaum 1989):

$$q(\zeta) = \frac{\pi\delta - 2p}{2p\delta - \pi}, \; p = \arctan\left[\varepsilon \tan\left(\frac{\pi\zeta}{2}\right)\right], \tag{44a,b}$$

with

$$\frac{d\xi}{dq} = \frac{(2p\delta - \pi)^2}{\pi^2\varepsilon(1-\delta^2)}\left[\cos^2\left(\frac{\pi\zeta}{2}\right) + \varepsilon^2 \sin^2\left(\frac{\pi\zeta}{2}\right)\right], \tag{45}$$

where $\varepsilon > 0$ and $|\delta| < 1$. The parameter ε controls the magnitude of the coordinate stretching about a point determined by the parameter δ. For $\zeta = \pm 1$, the amount of stretching is given by

$$\frac{d\xi}{dq} = \frac{1 \pm \delta}{1 \mp \delta}\varepsilon. \tag{46}$$

In this example, the parameters $\delta = 0$ and $\varepsilon = 0.3$, by which the high concentration of the gridpoints at the center of the mesh can be achieved. The grid spacing for the horizontal direction is $\Delta x = 10$ m, while the vertical grid spacing varies between $\Delta z_{\min} = 0.493$ m and $\Delta z_{\max} = 11.02$ m. The source is a point force emitting a Ricker signal and ω_c, t_s in eq. (15) are taken as 40π s^{-1} and 0.1 s, respectively. The angle between the direction of the force and x-axis is 45° and the force is applied at the horizontal gridpoint 51 ($x = 500$ m) and vertical grid 2($z = 0.493$ m). The calculation is carried out for a period of 0.9 s with a time step of 1.5×10^{-4} s by the second-order Euler predictor–corrector method and for all gridpoints $n_{G_p} = n_{G_s} = 10$, $n_{L_p} = n_{L_s} = 12$ and $c_p = c_s = 0.5$.

Figs 5(a)–(f) present single-trace comparisons of the results of the horizontal and vertical velocity between the PS method of the present paper and the transmitted-reflected-matrix (TRM) method (Apsel & Luco 1983; Luco & Apsel 1983; Pak & Guzina 2002). The three receivers (points 1, 2, 3) are located at (300, 188.38 m), (400, 188.38 m) and (400, 366.85 m), respectively. From Fig. 5, it follows that the match between the two solutions is very good.

Figs 6(a)–(d) show the vertical velocity snapshots of time 0.18, 0.27, 0.36 and 0.45 s, respectively. In the snapshot of Fig. 6(a), taken at an early time, only P, S and Rayleigh waves are visible.

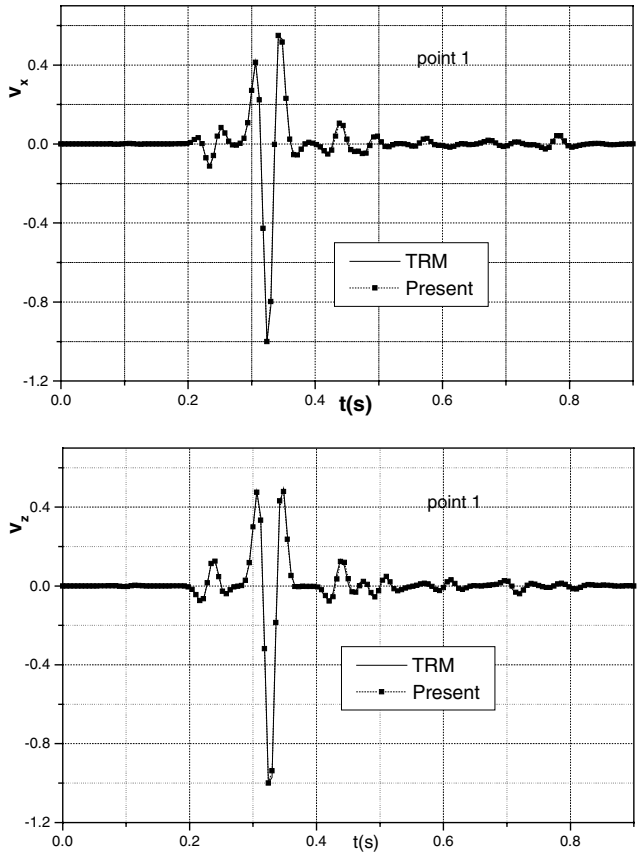

Figure 5. Comparison of the proposed method with the FFT method for the example B: (a) v_x at point 1, (b) v_z at point 1, (c) v_x at point 2, (d) v_z at point 2, (e) v_x at point 3, (f) v_z at point 3.

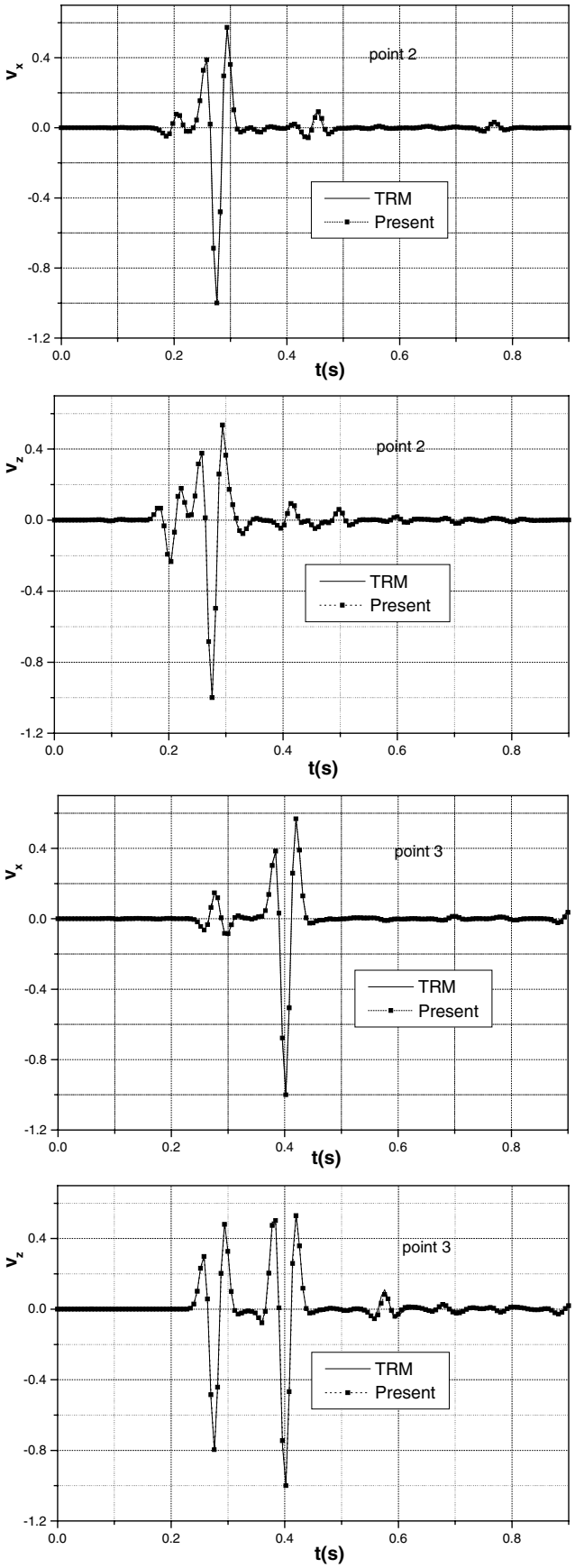

Figure 5. (*Continued.*)

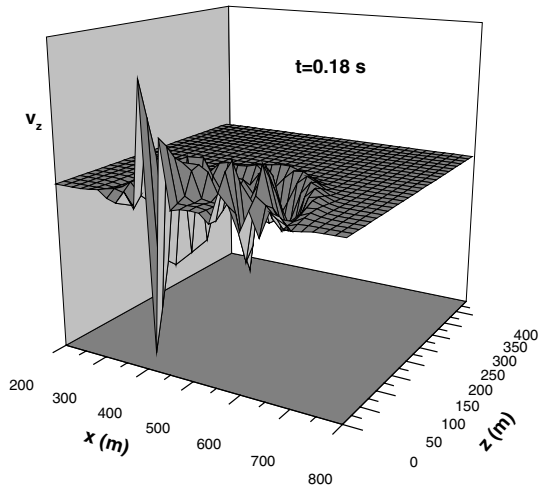

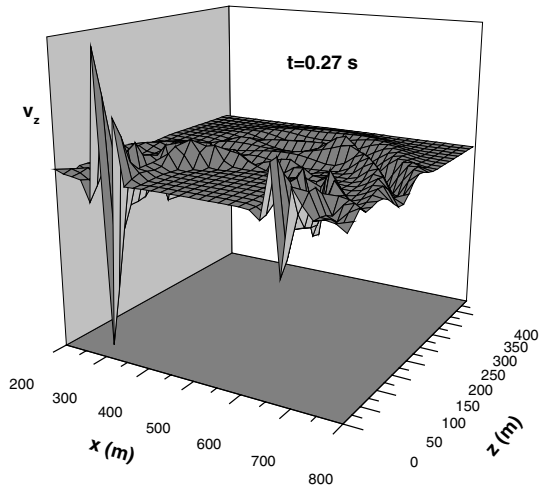

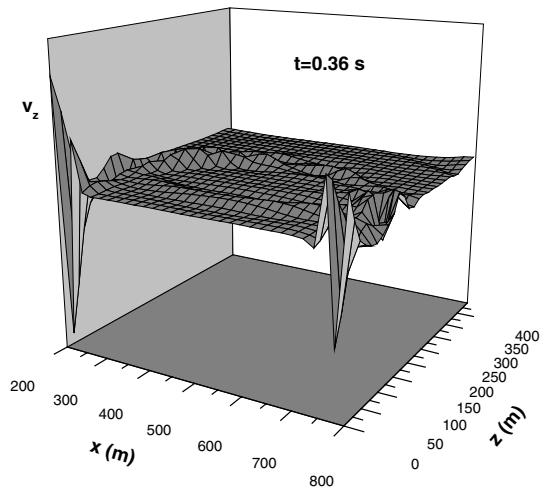

Figure 6. Snapshots of vertical velocity for the horizontal interface problem at: (a) $t = 0.18$ s, (b) $t = 0.27$ s, (c) $t = 0.36$ s, (d) $t = 0.45$ s.

In Fig. 6(b), the transmitted P and S waves are generated. In Fig. 6(c), the transmitted P wave is outside the domain and the transmitted S wave propagates in the half-space. The reflected wave in the layer is also visible. In Fig. 6(d), the Rayleigh wave is outside the calculation domain and the reflected wave from the free surface propagates in the layer.

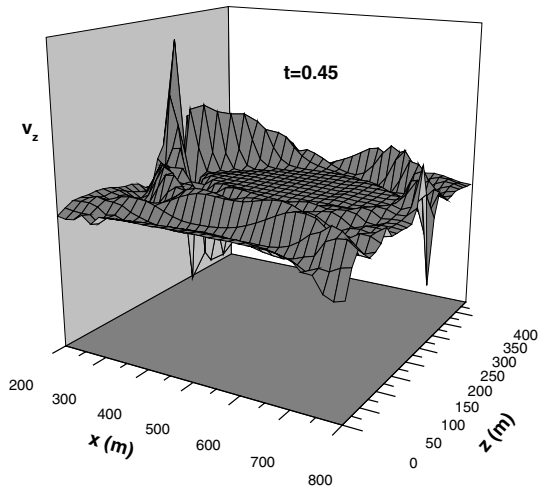

Figure 6. (*Continued.*)

5.3 Example C: viscoelastic medium with linear variation of the modulus

This example considers the viscoelastic half-space with linear variation of the viscoelastic modulus with increasing depth. The dimensions of the physical space are $x_{\max} = 1200$ m and $z_{\max} = 900$ m. For numerical calculation, grid size is 121 in the horizontal direction and 91 in the vertical direction with a free surface boundary condition at $z = 0$ and a non-reflecting boundary condition at $z = z_{\max}$. In order to eliminate the residual non-physical reflections, the absorbing strips of 20 grids are used at the lateral sides and the bottom of the calculation domain. The modulus of the viscoelastic medium are given by

$$M_{\infty p}(z) = M_{\infty p}(0) + \left[\Delta M_{\infty p}\frac{z}{z(N_z - 20)}\right], \tag{47a}$$

$$M_{\infty s}(z) = M_{\infty s}(0) + \left[\Delta M_{\infty s}\frac{z}{z(N_z - 20)}\right], \tag{47b}$$

where: $M_{\infty p}(0)$, $M_{\infty s}(0)$ are the moduli of the gridpoints at the free surface; $\Delta M_{\infty p}$, $\Delta M_{\infty s}$ are the difference of the modulus between the surface and the top of the absorbing strip; $z(N_z - 20)$ is the vertical coordinate of the points at the top of the absorbing strip. In this example, the material parameters are $M_{\infty p}(0) = 8.0 \times 10^9$ Pa, $M_{\infty s}(0) = 2.5 \times 10^9$ Pa, $\Delta M_{\infty p} = 1.0 \times 10^{10}$ Pa, $\Delta M_{\infty s} = 3.5 \times 10^9$ Pa, $\rho = 2000$ kg m^{-3}, $\eta_p = \eta_s = 0.1$ s, $a_p = a_s = 0.75$, $\alpha_p = \alpha_s = 0.5$. For the vertical coordinates z, the transformation (34) with $\alpha = 9.86$, $\beta = 0.5$ is applied. The grid size i horizontal direction is $\Delta x = 10$ m, while $\Delta z_{\min} = 0.934$ m, $\Delta z_{\max} = 10.95$ m, respectively. The source is a vertical point force emitting a Ricker signal with $\omega_c = 40\pi$ s^{-1} and $t_s = 0.1$ s, respectively. The force is applied at the horizontal gridpoint 26 ($x = 250$ m) and the vertical point 30 ($z = 230.6$ m). The calculation is carried out for a total propagation time of 1.2 s with a time step of 4.0×10^{-4} s by a second-order predictor-corrector method and for all gridpoints $n_{G_p} = n_{G_s} = 10$, $n_{L_p} = n_{L_s} = 12$ and $c_p = c_s = 0.5$.

Figs 7(a)–(d) show the vertical velocity snapshots of time 0.24, 0.48, 0.72 and 0.96 s. In Fig. 7(a), P and S waves are generated inside the viscoelastic medium and the Rayleigh wave develops along the free surface. In Fig. 7(b), P and S waves propagate in the viscoelastic medium while the Rayleigh wave propagates along the free surface. Moreover, the reflected P and S waves are generated inside the half-space. In Fig. 7(c), the direct P wave and S wave are

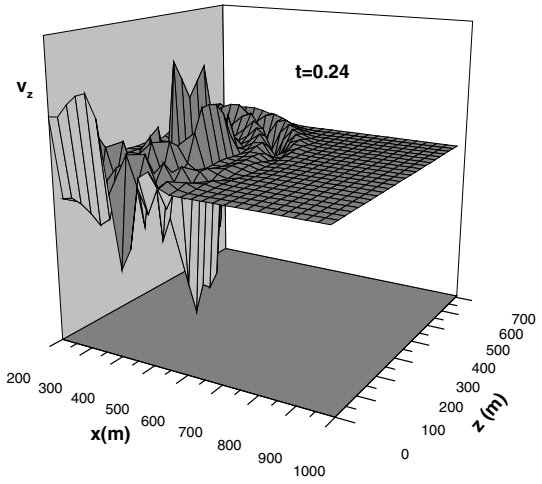

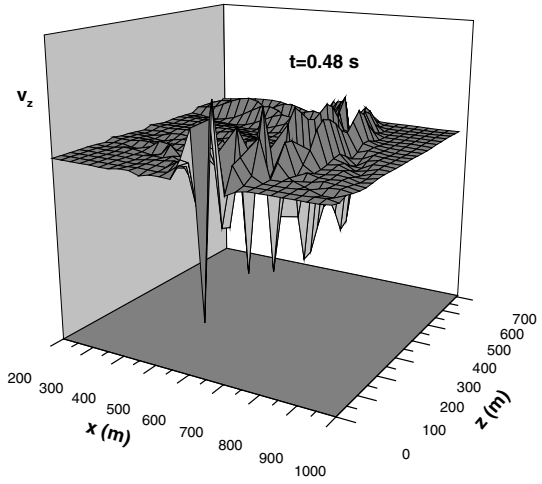

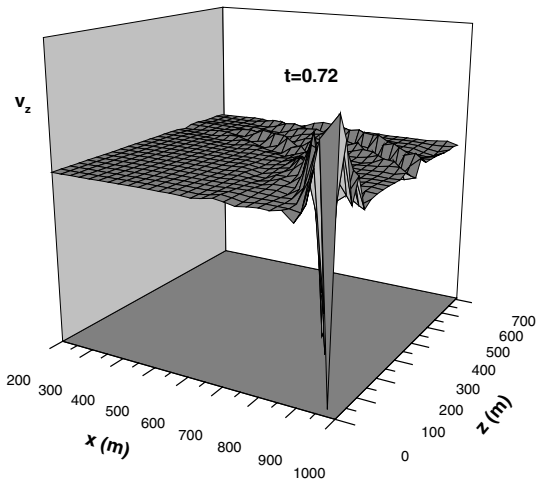

Figure 7. Snapshots of vertical velocity for the linear-variation modulus problem at: (a) $t = 0.24$ s, (b) $t = 0.48$ s, (c) $t = 0.72$ s, (d) $t = 0.96$ s.

outside the calculation domain, the reflected P waves and S waves are dominating inside the viscoelastic medium and the Rayleigh wave appears at the edge of the calculation domain. In Fig. 7(d), the Rayleigh wave has propagated outside the calculation domain and only the reflected waves remain.

Fig. 8 shows the seismograms for the horizontal and vertical velocities at the depth of $z = 0.934$ m. It shows clearly that the amplitudes of the P and S waves decrease rapidly with the increasing distance, while the amplitude of the Rayleigh wave decreases slowly. Also, at an early time, a non-causal signal appears near the vertical line through the source (Epperson 1987; Carcione 1996).

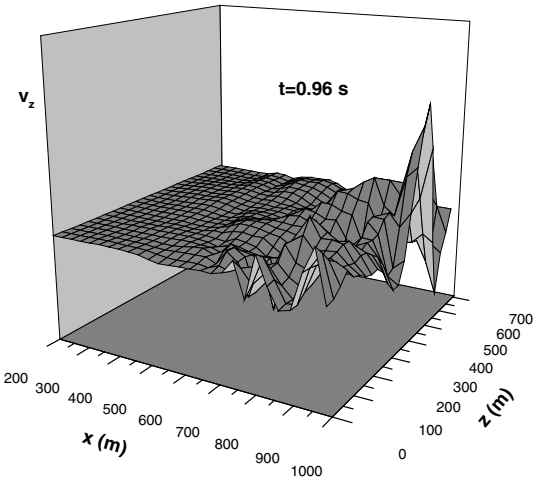

Figure 7. (*Continued.*)

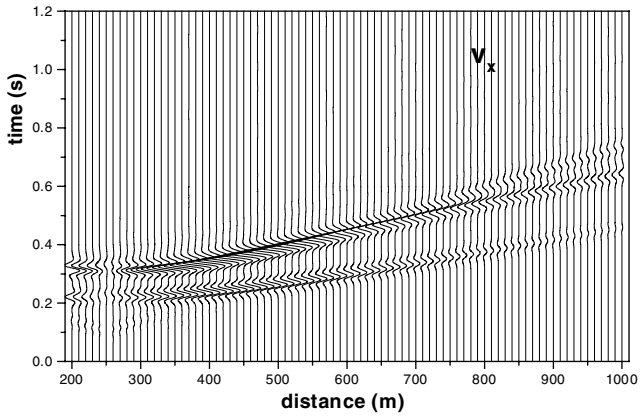

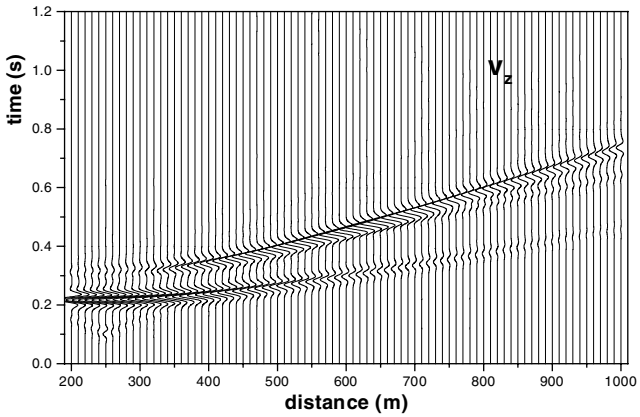

Figure 8. Seismograms for the velocity at the depth of $z = 0.934$ m: (a) horizontal velocity, (b) vertical velocity.

6 CONCLUSIONS

A new general modelling method for wave propagation in a linear viscoelastic medium with a singular memory has been developed in

the paper. Although the Cole–Cole law is used to characterize the viscoelastic medium of this paper, the proposed method also applies to an arbitrary viscoelastic medium with a singular memory. Obviously, the new method of solving fractional differential equations is also of importance for other applied engineering sciences involving the fractional differential equation $D^{\alpha}\chi(t) = f[\chi(t), t]$.

Our method of solving fractional differential equations reduces the fractional differential equations to a system of first-order differential equations, which avoids storage and integration of the entire variable histories. Thus, our approach is more economical than the methods based on a direct discretization of the fractional derivative. Moreover, the resulting first-order differential equations for the primary and secondary internal variables facilitate the implementation of the boundary condition and non-reflecting condition in the Chebychev PS method. The combination of the new method for solving fractional differential equations with the Fourier and Chebychev PS methods makes our method very efficient in term of computer storage, as a result of the fact that the Fourier and Chebychev PS method are accurate up to the maximum wavenumber of the mesh that corresponds to a spatial wavelength of two gridpoints.

It is also possible to construct internal variables with exponential relaxation directly using the relaxation spectrum representation of the stress relaxation function. This method, however, lead to a weight function that is sharply peaked and hence requires many quadrature points. The indirect method applied here based on the representation of a fractional derivative in terms of the secondary internal variables, involves a monotonically decreasing weight function and, therefore, requires a small number of quadrature points.

By using the coordinate transformation method, the dynamic response of curved surface topographies of a singular memory viscoelastic medium can also be solved by our method. Also, extension of our method to the 3-D wave propagation in a viscoelastic medium with a singular memory is straightforward. Moreover, material anisotropy can be easily incorporated in our method (Hanyga 2003a). The proposed method can be used in solving the Biot's poroelastic medium with a singular memory involved in the drag force.

ACKNOWLEDGMENTS

The research is financed by the Norwegian Scientific Council in the framework of the project 149238/431 'Mathematical formulation of seismic attenuation based on physical models of mechanical rock behaviour'. Valuable advices from José Carcione, Robert Graves and an anonymous reviewer are greatly appreciated.

REFERENCES

Achenbach, J.D., 1973. *Wave Propagation in Elastic Solids,* North-Holland, Amsterdam.

Apsel, R.J. & Luco, J.E., 1983. On the Green's functions for a layered half-space: Part II, *Bull. seism. Soc. Am.,* **73,** 931–951.

Augenbaum, J.M., 1989. An adaptive pseudospectral method for discontinuous problems, *Appl. Numer. Math.,* **5,** 459–480.

Bagley, R.L. & Torvik, P.J., 1983. A theoretical basis for the application of fractional calculus to viscoelasticity, *J. Rheol.,* **27,** 201–210.

Bagley, R.L. & Torvik, P.J., 1986. On the fractional calculus model of viscoelastic behavior, *J. Rheol.,* **30,** 133–155.

Batzle, M., Hofmann, R., Han, D.H. & Castagna, J., 2001. Fluids and frequency dependent seismic velocity of rocks, *The Leading Edge,* **20,** 168–171.

Borcherdt, R.D., 1982. Reflection-refraction of general P- and type-II S waves in elastic and anelastic solids, *Geophys. J. R. astr. Soc.,* **70,** 621–638.

Borcherdt, R.D. & Wenneberg, L., 1985. General P, type-I S, and type-II S waves in anelastic solids; inhomogeneous waves fields in low-loss solids, *Bull. seism. Soc. Am.,* **75,** 1729–1763.

Carcione, J.M., 1996. A 2D Chebyshev differential operator for the elastic wave equation, *Comput. Meth. Appl. Mech. Eng.,* **130,** 33–45.

Carcione, J.M., 2001. *Wave Fields in Real Media: Wave Propagation in Anisotropic, Anelastic, and Porous Media,* Pergamon, Amsterdam.

Carcione, J.M., Kosloff, D. & Kosloff, R., 1988. Wave propagation simulation in a linear viscoelastic medium, *Geophys. J.,* **95,** 597–611.

Christensen, R.M., 1971. *Theory of viscoelasticity: An introduction,* Academic Press, New York.

Cole, K.S. & Cole, R.H., 1941. Dispersion and absorption in dielectrics, I: Alternating current characteristics, *J. Chem. Phys.,* **9,** 341–351.

Davis, P.J. & Rabinowitz, P., 1984. *Method of Numerical Integration,* Academic Press, Inc., Orlando, FL.

Day, S.M. & Minster, J.B., 1984. Numerical-simulation of attenuated wavefields using a pade approximant method., *Geophys. J. R. astr. Soc.,* **78,** 105–118.

Diethelm, K., Ford, N.J. & Freed, A.D., 2002. A predictor-corrector approach for the numerical solution of fractional differential equations, *Nonlinear Dyn.,* **29,** 3–22.

Emmerich, H. & Korn, M., 1987. Incorporation of attenuation into time-domain computations of seismic-wave fields, *Geophysics,* **52,** 1252–1264.

Enelund, M. & Olsson, P., 1999. Damping described by fading memory—analysis and application to fractional derivative models, *Int. J. Solids Structures,* **36,** 939–970.

Epperson, J.F., 1987. On the Runge example, *Am. Math. Mon.,* **94,** 329–341.

Friedrich, C. & Braun, H., 1994. Linear viscoelastic behavior of complex polymeric materials—a fractional mode representation, *Colloid Polym. Sci.,* **272,** 1536–1546.

Fung, Y.C., 1965. *Foundations of solid mechanics,* Prentice-Hall, Englewood Cliffs, NJ.

Futterman, W., 1962. Dispersive body wave, *J. geophys. Res.,* **67,** 5279–5291.

Glöckle, W.G. & Nonnenmacher, T.F., 1991. Fractional integral-operators and Fox functions in the theory of viscoelasticity, *Macromolecules,* **24,** 6426–6434.

Gorenflo, R. & Mainardi, F., 1997. Fractional Calculus: integral and differential equations of fractional order, in *Fractals and Fractional Calculus in Continuum Mechanics,* pp 223–276, eds Carpinteri, A. & Mainardi, F., Springer Verlag, Vienna and New York.

Gottlieb, D. & Orszag, S., 1977. *Numerical Analysis of Spectral Method, Theory and Application,* Society for Industrial and Applied Mathematics, Philadelphia.

Gottlieb, D., Gunzberger, M.D. & Turkel, E., 1982. On numerical boundary treatment for hyperbolic systems, *SIAM J. Num. Anal.,* **19,** 671–682.

Hanyga, A., 2003a. An anisotropic Cole–Cole model of seismic attenuation, *J. Comput. Acoust.,* **11,** 75–90.

Hanyga, A., 2003b. Internal variable models of viscoelasticity with fractional relaxation law, DETC 2003/VIB-48395.

Hanyga, A. & Seredyńska, M., 1999. Some effects of the memory kernel singularity on wave propagation and inversion in poroelastic media, I: Forward modeling, *Geophys. J. Int.,* **137,** 319–335.

Jones, T.D., 1986. Pore fluids and frequency-dependent wave propagation in rocks, *Geophysics,* **51,** 1939–1953.

Kjartansson, E., 1979. Constant-Q wave propagation and attenuation, *J. geophys. Res.,* **84,** 4737–4748.

Kosloff, R. & Kosloff, D., 1986. Absorbing boundaries for wave propagation problems, *J. Comput. Phys.,* **63,** 363–376.

Kosloff, D. & Tal-Ezer, H., 1993. A modified Chebyshev pseudospectral method with an $O(N^{-1})$ time step restriction, *J. Comput. Phys.,* **104,** 457–469.

Kosloff, D., Kessler, D., Quieroz, A., Tessmer, E., Behle, A. & Strahilevitz, R., 1990. Solution of the equations of dynamic elasticity by a Chebychev spectral method, *Geophysics,* **55,** 734–748.

Luco, J.E. & Apsel, R.J., 1983. On the Green's functions for a layered half-space: Part I, *Bull. seism. Soc. Am.,* **73,** 909–929.

Nolte, B., Kempe, S., & Schafer, I., 2003. Does a real material behave fractionally? Applications of fractional differential operators to the damped strucure borne sound in viscoelastic solids, *J. Comput. Acoustics,* **11,** 451–489.

Oppenheim, A.V. & Schafer, R.W., 1999. *Discrete-time signal processing,* Prentice-Hall, Inc., Englewood Cliffs, NJ.

Padovan, J., 1987. Computational algorithm for finite element formulation involving fractional operator, *Compu. Mech.,* **2,** 275–282.

Pak, R.Y.S. & Guzina, B.B., 2002. Three-dimensional Green's functions for a multilayered half-space in displacement potentials, *J. Eng. Mech.,* **128,** 449–461.

Papoulis, A., 1962. *The Fourier integral and its application,* McGraw-Hill, New York.

Podlubny, I., 1998. *Fractional differential equations,* Academic Press, San Diego.

Rabotnov, Y.N., 1980. *Elements of hereditary solid mechanics,* Mir Publication, Moscow.

Ricker, N.H., 1977. *Transient Waves in Visco-elastic Media,* Elsevier, Amsterdam.

Soula, M., Vinh, T. & Chevalier, Y., 1997. Transient responses of polymers and elastomers deduced from harmonic responses, *J. Sound Vibr.,* **205,** 185–203.

Strick, E., 1970. A predicted pedestal effect for a pulse propagating in constant Q solids, *Geophysics,* **35,** 387–403.

Thompson, K.W., 1990. Time-dependent boundary conditions for hyperbolic systems, II, *J. Comp. Phys.,* **89,** 439–461.

Xu, T. & Mcmechan, G.A., 1995. Composite memory variables for viscoelastic synthetic seismograms, *Geophy. J. Int.,* **121,** 634–639.

Yuan, L. & Agrawal, O.P., 2002. A numerical scheme for dynamic systems containing fractional derivatives, *J. Vib. Acoust.,* **124,** 321–324.

APPENDIX A: VECTORS AND THE MATRIX IN EQ. (26A)

The unknown variable vector **V** in eq. (26a) is given by the following expression:

$$\mathbf{V} = \left[v_x, v_z, \sigma_{xx}, \sigma_{zz}, \sigma_{zx}, \chi^p_{zx}, \chi^s_{xx}, \chi^s_{zz}, \chi^s_{zx}, \langle \phi^p_{zx_i} \rangle_{N^p_I}, \langle \phi^s_{xx_i} \rangle_{N^s_I}, \langle \phi^s_{zz_i} \rangle_{N^s_I}, \langle \phi^s_{zx_i} \rangle_{N^s_I} \right]^T . \tag{A1a}$$

Matrix **A** and **B** in eq. (26a) are given by

$$\mathbf{A} = \begin{bmatrix}
0 & 0 & \rho^{-1} & 0 & 0 & \ldots\ldots 0 \\
0 & 0 & 0 & 0 & \rho^{-1} & \ldots\ldots 0 \\
M_{\infty p} & 0 & 0 & 0 & 0 & \ldots\ldots 0 \\
M_{\infty p} - 2M_{\infty s} & 0 & 0 & 0 & 0 & \ldots\ldots 0 \\
0 & M_{\infty s} & 0 & 0 & 0 & \ldots\ldots 0 \\
\delta_p & 0 & 0 & 0 & 0 & \ldots\ldots 0 \\
\delta_s & 0 & 0 & 0 & 0 & \ldots\ldots 0 \\
0 & 0 & 0 & 0 & 0 & \ldots\ldots 0 \\
0 & \delta_s & 0 & 0 & 0 & \ldots\ldots 0 \\
\delta_p y_{p_i}^{2\alpha_p - 1} & 0 & 0 & 0 & 0 & \ldots\ldots 0, \\
i = 1, \ldots, N^p_I & & \vdots & & & \\
\delta_s y_{s_i}^{2\alpha_s - 1} & 0 & 0 & 0 & 0 & \ldots\ldots 0, \\
i = 1, \ldots, N^s_I & & \vdots & & & \\
0 & 0 & 0 & 0 & 0 & \ldots\ldots 0, \\
i = 1, \ldots, N^s_I & & \vdots & & & \\
0 & \delta_s y_{s_i}^{2\alpha_s - 1} & 0 & 0 & 0 & \ldots\ldots 0, \\
i = 1, \ldots, N^s_I & & \vdots & & &
\end{bmatrix}
\begin{matrix} \\ \\ \\ \\ \\ \\ \\ \\ \\ \Big\} N^p_I \\ \\ \Big\} N^s_I \\ \\ \Big\} N^s_I \\ \\ \Big\} N^s_I \end{matrix}$$

$$, \mathbf{B} = \begin{bmatrix}
0 & 0 & 0 & 0 & \rho^{-1} & \ldots\ldots 0 \\
0 & 0 & 0 & \rho^{-1} & 0 & \ldots\ldots 0 \\
0 & M_{\infty p} - 2M_{\infty s} & 0 & 0 & 0 & \ldots\ldots 0 \\
0 & M_{\infty p} & 0 & 0 & 0 & \ldots\ldots 0 \\
M_{\infty s} & 0 & 0 & 0 & 0 & \ldots\ldots 0 \\
0 & \delta_p & 0 & 0 & 0 & \ldots\ldots 0 \\
0 & 0 & 0 & 0 & 0 & \ldots\ldots 0 \\
0 & \delta_s & 0 & 0 & 0 & \ldots\ldots 0 \\
\delta_s & 0 & 0 & 0 & 0 & \ldots\ldots 0 \\
0 & \delta_p y_{p_i}^{2\alpha_p - 1} & 0 & 0 & 0 & \ldots\ldots 0, \\
i = 1, \ldots, N^p_I & & \vdots & & & \\
0 & 0 & 0 & 0 & 0 & \ldots\ldots 0, \\
i = 1, \ldots, N^s_I & & \vdots & & & \\
0 & \delta_s y_{s_i}^{2\alpha_s - 1} & 0 & 0 & 0 & \ldots\ldots 0, \\
i = 1, \ldots, N^s_I & & \vdots & & & \\
\delta_s y_{s_i}^{2\alpha_s - 1} & 0 & 0 & 0 & 0 & \ldots\ldots 0, \\
i = 1, \ldots, N^s_I & & \vdots & & &
\end{bmatrix}
\begin{matrix} \\ \\ \\ \\ \\ \\ \\ \\ \\ \Big\} N^p_I \\ \\ \Big\} N^s_I \\ \\ \Big\} N^s_I \\ \\ \Big\} N^s_I \end{matrix} .$$

(A1b,c)

Vector **C** in eq. (26a) is given by

$$\mathbf{C} = \Bigg[\frac{f_x}{\rho}, \frac{f_y}{\rho}, \chi^p_{zx} - 2\chi^s_{zz}, \chi^p_{zx} - 2\chi^s_{xx}, \chi^s_{zx}, -\frac{\kappa_p}{\Psi_{L_p}} \sum_{i=1}^{N_I^p} w_{p_i} \phi^p_{zx_i} - \frac{\eta_p^{\alpha_p} \Psi_{G_p} + 1}{\Psi_{L_p} \eta_p^{\alpha_p}} \chi^p_{zx},$$

$$-\frac{\kappa_s}{\Psi_{L_s}} \sum_{i=1}^{N_I^s} w_{s_i} \phi^s_{xx_i} - \frac{\eta_s^{\alpha_s} \Psi_{G_s} + 1}{\Psi_{L_s} \eta_s^{\alpha_s}} \chi^s_{xx}, -\frac{\kappa_s}{\Psi_{L_s}} \sum_{i=1}^{N_I^s} w_{s_i} \phi^s_{zz_i} - \frac{\eta_s^{\alpha_s} \Psi_{G_s} + 1}{\Psi_{L_s} \eta_s^{\alpha_s}} \chi^s_{zz},$$

$$-\frac{\kappa_s}{\Psi_{L_s}} \sum_{i=1}^{N_I^s} w_{s_i} \phi^s_{zx_i} - \frac{\eta_s^{\alpha_s} \Psi_{G_s} + 1}{\Psi_{L_s} \eta_s^{\alpha_s}} \chi^s_{zx}, \left\langle -y_{p_i}^2 \phi^p_{zx_i} - \frac{y_{p_i}^{2\alpha_p - 1} \kappa_p}{\Psi_{L_p}} \sum_{j=1}^{N_I^p} w_{p_j} \phi^p_{zx_j} \right.$$

$$\left. - \frac{y_{p_i}^{2\alpha_p - 1} (\eta_p^{\alpha_p} \Psi_{G_p} + 1)}{\Psi_{L_p} \eta_p^{\alpha_p}} \chi^p_{zx} \right\rangle_{N_I^p}, \left\langle -y_{s_i}^2 \phi^s_{xx_i} - \frac{y_{s_i}^{2\alpha_s - 1} \kappa_s}{\Psi_{L_s}} \sum_{j=1}^{N_I^s} w_{s_j} \phi^s_{xx_j} - \frac{y_{s_i}^{2\alpha_s - 1} \left(\eta_s^{\alpha_s} \Psi_{G_s} + 1\right)}{\Psi_{L_s} \eta_s^{\alpha_s}} \chi^s_{xx} \right\rangle_{N_I^s},$$

$$\left\langle -y_{s_i}^2 \phi^s_{zz_i} - \frac{y_{s_i}^{2\alpha_s - 1} \kappa_s}{\Psi_{L_s}} \sum_{j=1}^{N_I^s} w_{s_j} \phi^s_{zz_j} - \frac{y_{s_i}^{2\alpha_s - 1} (\eta_s^{\alpha_s} \Psi_{G_s} + 1)}{\Psi_{L_s} \eta_s^{\alpha_s}} \chi^s_{zz} \right\rangle_{N_I^s},$$

$$\left\langle -y_{s_i}^2 \phi^s_{zx_i} - \frac{y_{s_i}^{2\alpha_s - 1} \kappa_s}{\Psi_{L_s}} \sum_{j=1}^{N_I^s} w_{s_j} \phi^s_{zx_j} - \frac{y_{s_i}^{2\alpha_s - 1} (\eta_s^{\alpha_s} \Psi_{G_s} + 1)}{\Psi_{L_s} \eta_s^{\alpha_s}} \chi^s_{zx} \right\rangle_{N_I^s} \Bigg]^T, \tag{A1d}$$

where: v_x, v_z, σ_{xx}, σ_{zz}, σ_{zx} and χ^p_{zx}, χ^s_{xx}, χ^s_{zz}, χ^s_{zx} are the velocities, stresses and primary internal variables respectively; $\phi^p_{zx_i}, i = 1, 2, \ldots, N_I^p, \phi^s_{xx_i}, \phi^s_{zz_i}, \phi^s_{zx_i}$, $i = 1, 2, \ldots, N_I^s$ are the secondary internal variables corresponding to χ^p_{zx}, χ^s_{xx}, χ^s_{zz}, χ^s_{zx}, respectively; N_I^p, N_I^s are the total quadrature points for the exponents α_p and α_s; and $N_I^p = n_{G_p} + n_{L_p}$, $N_I^s = n_{G_s} + n_{L_s}$; $\langle \cdot \rangle_N$ denotes a set of N elements. Besides,

$$\kappa_p = \frac{2\sin(\pi\alpha_p)}{\pi}, \quad \kappa_s = \frac{2\sin(\pi\alpha_s)}{\pi}, \quad \Psi_{G_p} = \kappa_p \left[\frac{c_p^{2\alpha_p}}{2\alpha_p} - \sum_{i=1}^{n_{G_p}} w_{p_i}^G \left(y_{p_i}^G\right)^{2\alpha_p - 1} \right], \tag{A2a,b,c}$$

$$\Psi_{G_s} = \kappa_s \left[\frac{c_s^{2\alpha_s}}{2\alpha_s} - \sum_{i=1}^{n_{G_s}} w_{s_i}^G \left(y_{s_i}^G\right)^{2\alpha_s - 1} \right], \quad \Psi_{L_p} = \kappa_p \left[\frac{c_p^{2\alpha_p - 2}}{2 - 2\alpha_p} - \sum_{i=1}^{n_{L_p}} w_{p_i}^L \left(y_{p_i}^L\right)^{2\alpha_p - 3} \right], \tag{A2d,e}$$

$$\Psi_{L_s} = \kappa_s \left[\frac{c_s^{2\alpha_s - 2}}{2 - 2\alpha_s} - \sum_{i=1}^{n_{L_s}} w_{s_i}^L \left(y_{s_i}^L\right)^{2\alpha_s - 3} \right], \quad \delta_p = \frac{M_{\infty p}(a_p - 1)}{\Psi_{L_p} \eta_p^{\alpha_p}}, \quad \delta_s = \frac{M_{\infty s}(a_s - 1)}{\Psi_{L_s} \eta_s^{\alpha_s}}, \tag{A2f,g,h}$$

where: n_{G_p}, $w_{p_i}^G$, $y_{p_i}^G$, $i = 1, 2, \ldots, n_{G_p}$ denote the number of the Gauss quadrature points, the corresponding weights and the abscissas for the exponent α_p, and n_{G_s}, $w_{s_i}^G$, $y_{s_i}^G$, $i = 1, 2, \ldots, n_{G_s}$ are the similar variables for the exponent α_s; n_{L_p}, $w_{p_i}^L$, $y_{p_i}^L$, $i = 1, 2, \ldots, n_{L_p}$ are the quadrature point number, the weights and the abscissas in the shifted Laguerre quadrature formula for the exponent α_p, and n_{L_s}, $w_{s_i}^L$, $y_{s_i}^L$, $i = 1, 2, \ldots, n_{L_s}$ are those for the exponent α_s; $w_{p_i}, y_{p_i}, i = 1, 2, \ldots, N_{I\,p}$ are the combinations of $w_{p_i}^G, y_{p_i}^G, i = 1, 2, \ldots, n_{G_p}$ and $w_{p_i}^L, y_{p_i}^L$, $i = 1, 2, \ldots, n_{L_p}$ as defined in eq. (24b,c) and N_I^s, $w_{s_i}, y_{s_i}, i = 1, 2, \ldots, N_I^s$ are the similar variables for the exponent α_s.